Supplementary file 1

for

The evolution of mitogenomic architecture in Bilateria

by

Dong Zhang, Yi-Wen Ma, Tong Ye, Rui Han, Xiang Liu, Hong Zou, Jin Zhang, Rui Song, Gui-Tang Wang, Fei Liu, Benhe Zeng, Jinsong Chen, Ivan Jakovlić

* Corresponding author: Ivan Jakovlić (jakovlici@lzu.edu.cn)

Contents

Table S1. The list of mitogenomes sequenced by our research team(s).

No	Species	Phylum	Publication
1	*Tetraonchus monenteron*	Platyhelminthes	[1]
2	*Enterogyrus malmbergi*	Platyhelminthes	[2]
3	*Lamellodiscus spari*	Platyhelminthes	[3]
4	*Lepidotrema longipenis*	Platyhelminthes	[3]
5	*Sindiplozoon* sp.	Platyhelminthes	[4]
6	*Eudiplozoon* sp.	Platyhelminthes	[4]
7	*Paradiplozoon opsariichthydis*	Platyhelminthes	[4]
8	*Paratetraonchoides inermis*	Platyhelminthes	[5]
9	*Dactylogyrus lamellatus*	Platyhelminthes	[6]
10	*Thaparocleidus asoti*	Platyhelminthes	[7]
11	*Thaparocleidus varicus*	Platyhelminthes	[7]
12	*Euryhaliotrema johni*	Platyhelminthes	[8]
13	*Gangesia oligonchis*	Platyhelminthes	[9]
14	*Atractolytocestus huronensis*	Platyhelminthes	[10]
15	*Khawia sinensis*	Platyhelminthes	[10]
17	*Breviscolex orientalis*	Platyhelminthes	[10]
18	*Schyzocotyle acheilognathi*	Platyhelminthes	[10]
19	*Digramma interrupta*	Platyhelminthes	[11]
20	*Ligula intestinalis*	Platyhelminthes	[11]
21	*Gyrodactylus gurleyi*	Platyhelminthes	[12]
22	*Gyrodactylus* sp. L1	Platyhelminthes	[13]
23	*Gyrodactylus* sp. L4	Platyhelminthes	[13]
24	*Diplorchis* sp.	Platyhelminthes	[14]
25	*Gyrodactylus kobayashii*	Platyhelminthes	[15]
26	*Dollfustrema vaneyi*	Platyhelminthes	[16]
27	*Aspidogaster conchicola*	Platyhelminthes	work in progress
28	*Aspidogaster ijimai*	Platyhelminthes	work in progress
29	*Diceratocephala sp.*	Platyhelminthes	work in progress
30	*Craspedella pedum*	Platyhelminthes	work in progress
31	*Pseudocapillaria tomentosa*	Nematoda	[17]
32	*Camallanus lacustris*	Nematoda	[18]
33	*Clavinema parasiluri*	Nematoda	[18]
34	*Philometra sp.*	Nematoda	[18]
35	*Camallanus cotti*	Nematoda	[19]
36	*Pingus sinensis*	Nematoda	[20]
37	*Eustronglylides ignotus*	Nematoda	work in progress
38	*Procamallanus fulvidraconis*	Nematoda	work in progress
39	*Rhabdochona sp.*	Nematoda	work in progress
40	*Cucullanus cyprini*	Nematoda	work in progress
41	*Camallanus hypophthalmichthys*	Nematoda	work in progress
42	*Cymothoa indica*	Arthropoda	[21]
43	*Asotana magnifica*	Arthropoda	[22]
44	*Tachaea chinensis*	Arthropoda	[23]
45	*Ichthyoxenos japonensis*	Arthropoda	[23]

Text S1. Overview of hypotheses

1) The ancestral mitogenomic architecture of Bilateria is **(a)** identical to the one exhibited by most vertebrates (ur-Vertebrata), and **(b)** double-stranded.

2) Single-stranded (all genes encoded on one strand) to double-stranded (genes encoded on both strands) architecture type evolutionary shifts are non-existent.

3) Mitogenomic architecture evolution is episodic (often re-stabilised after an evolutionary period of smaller or greater architectural rearrangements, commonly occurring deep in the evolutionary history) and discontinuous (in most phyla, the ancestral architecture for the phylum is highly conserved in a majority of species, with exponentially elevated rearrangement rates in a small proportion of species.

4) The correlation between the architectural evolution (GORR) and sequence evolution (branch length) is **(a)** positive, **(b)** but only in lineages with highly rearranged mitogenomic architectures (GORR≥7), **(c)** and only in lineages with double-stranded architectures.

5) Lineages with a single-stranded architectures exhibit higher **(a)** architecture (GORR) and **(b)** sequence (branch length) evolutionary rates.

6) Compared to free-living species, parasitic species exhibit elevated **(a)** GORR values, **(b)** with the effect persisting when variability in locomotory capacity is accounted for (the hypothesis tested using only Low locomotory capacity category). **(c)** Single-stranded architectures are statistically overrepresented in parasitic species.

7) Compared to high-locomotory species, low-locomotory species exhibit elevated: **(a)** GORR values, **(b)** with the effect persisting when variability in lifestyle is removed from the dataset (the hypothesis tested using only free-living species). **(c)** Single-stranded architectures are statistically overrepresented in low-locomotory species.

8) There is a positive correlation between the mitogenome size and **(a)** architecture (GORR), and **(b)** sequence (branch length) evolutionary rates. Mitogenomic sizes are increased in **(c)** parasitic species and **(d)** low-locomotory species.

Text S2. Additional methodological details

The pipeline to resolve duplicated genes (i.e. leave only the ancestral copy), was designed by us for a previous study [24] and implemented in PhyloSuite v1.2.3 [25]. Briefly, the pipeline first searches for the existence of stop codons in gene duplicates, and then removes the one possessing them, as this implies non-functionality. If this step does not resolve the duplicates, then it compares the orthologous genes of the closest available taxon in the dataset, and keeps the most conserved duplicate.

We adopted the definition of parasitism as a consumer interaction in which the consumer feeds on a single individual (the host) during at least one life-history stage, where both parasites and hosts belong to the Animalia. This includes strategies employed by parasitoids, parasitic castrators, macroparasites and pathogens, but excludes micropredators, brood parasites, kleptoparasites, symbiotic egg predators, inquilines, non-feeding symbionts, and plant-parasites [24,26,27]. Parasites living inside the host's body were classified as endoparasites (this category also included mesoparasites) (274 species). Parasites attaching themselves to or permanently living on the surface of the host's body were classified as ectoparasites (117 species). We found before that endoparasites exhibit higher evolutionary rates than ectoparasites, and attributed it to their lower locomotory capacity and higher metabolic dependence on the host [24]. Parasitoids (66 species) comprise organisms that are parasitic during a part of their life cycle (commonly this comprises a parasitic larva stage), followed by a free-living adult stage. As such, they evolve under a stronger purifying selection pressure than ecto- and endo-parasites, and exhibit lower mitogenomic evolutionary rates [24]. We also separately classified micropredators (186 species), as they resemble many ectoparasites in their haematophagous feeding habits, but they only visit the host for feeding (e.g. mosquitoes). All other bilaterian species were classified as free-living (10,217 species). For further details about these classifications and sequence evolutionary rates see [24].

The categorisation of locomotory capacity was based on the "visual interaction hypothesis", which is the best explanatory variable for variability in scaling coefficients between the mass-specific metabolic rate in marine animals: high metabolic demand follows strong selection for locomotory capacity for pursuit and evasion in visual prey/predators inhabiting well-lit oceanic waters, whereas limited visibility allows for reduced locomotory capacity, reflected in low metabolic rates [28,29]. We divided the dataset into three locomotory capacity categories: (1) High comprised all species expected to rely on locomotion for pursuit and evasion of prey/predators. This category comprised a vast majority of species (8,713); (2) Low comprised all species that have merely a rudimentary locomotory capacity. This comprises sedentary species, or those capable only of minimal, very slow locomotion, that do not

rely on locomotion for pursuit and evasion of prey/predators. This category comprised 1,202 species, mostly from lineages such as nematodes, flatworms, sessile molluscs and crustaceans, parasitic crustaceans, ticks, some annelids, mites, Acanthocephala, Diplura, Brachiopoda, Bryozoa, Ascidiacea, Echinodermata, Entoprocta, Gastrotricha, Gnathostomulida, Hemichordata, Kinorhyncha, Nemertea, Onychophora, Orthonectida, Phoronida, Priapulida, Tardigrada, and Xenacoelomorpha; (3) Because locomotory capacity is a continuous trait, it is impossible to categorise species into only two categories without creating a large overlap between the two categories. Therefore, to minimise the overlap between the Low and High locomotory capacity categories, we designed a third category: Intermediate locomotory capacity. This category comprised 945 species that would be expected to possess more than a rudimentary locomotory capacity, but also rely on strategies other than locomotion to evade/pursue predators/prey. Examples are certain flightless insects and Collembola, certain bathyal, abyssal and stygobitic crustacean and fish lineages, Chaetognatha, certain amphibian and reptilian lineages, some mammals, some Bivalvia and Cephalopoda, some Gastropoda, Nematomorpha, and Rotifera.

All steps of phylogenetic analyses were conducted using PhyloSuite [25,30] and its plug-in programs. All gene sequences were aligned using MAFFT v7.475 [31], alignments trimmed by trimAl v1.2rev59 [32], and concatenated by PhyloSuite.

For the inference of ancestral architecture, we also tested ProCARs [33], but the results were nonsensical (details in Text S3), so we discarded them as unreliable. Additional analyses were conducted using MLGO and all genes (tRNAs included) to infer the ancestral state of Lophotrochozoa. As the outgroup for this analysis, we used two Ecdysozoa species: *Priapulus caudatus* (Priapulida) and *Limulus polyphemus* (Arthropoda), as their architectures are separated by a single rearrangement event [34]. The "Xenambulacraria" topology was constrained according to [35,36] as follows: (Porifera,(Placozoa,(Cnidaria,(Chordata,(Xenacoelomorpha,(Echinodermata,Hemichordata))))))). Ctenophora was excluded due to missing genes.

The main dataset (10,860 mitogenomes) comprised only those from the curated NCBI's RefSeq database [37], which comprises only complete mitogenomes manually confirmed by the GenBank staff, and only one per species. The full GenBank dataset commonly also comprises multiple mitogenomes per species, those flagged as "unconfirmed" by the GenBank staff, incomplete, unannotated/partially annotated, etc.

Three different effect size measures were used. Cohen's d should be used when the two groups have similar standard deviations and the same sample size that is >20. Glass's Δ should be used when the

two groups' standard deviations are different. Hedges's g should be used when the two groups have similar standard deviations and different sample sizes, or both groups have a sample size <20 per group. Cohen's d values can be interpreted in the following way: d<0.2 = small effect size, 0.2<d<0.5 = medium, 0.5<d<0.8 = large, and d>0.8 = very large. Statistical power analyses were conducted for each effect size measure using pwr.t2n.test method in the R package 'pwr'. Power refers to the probability of detecting a statistically significant effect if one exists, where the commonly accepted cut-off value for a good statistical power is ≥ 0.8.

Table S2. Previous proposals for ancestral architectures of selected lineages.

Ancestral for	**References**
Bilateria	[38,39]
Deuterostomia	[40]
Ecdysozoa	[34]
Arthropoda	[39,41]
Mollusca	[42]
Gastropoda	[39]

Table S3. Details for Figure 1 in the main manuscript. No is species count; s-s is the number of single-stranded mitogenomes; d-s is the number of double-stranded mitogenomes; GORR is gene order rearrangement rate; Size is mitogenome size in base pairs; BRL is branch length; SD is standard deviation.

Phylum	No	s-s	d-s	GORR		Size		BRL	
				mean	SD	mean	SD	mean	SD
Chordata	6226	25	6201	0.2	0.52	16791.89	660.44	1.97	0.26
Arthropoda	3476	4	3472	3.17	0.66	15726.04	1160.07	2.9	0.67
Mollusca	551	119	432	6.93	2.39	16351.47	2750.8	3.58	1.25
Nematoda	174	148	26	5.71	1.23	14426.52	1727.97	6.84	0.77
Platyhelminthes	149	148	1	8.74	0.78	14380.99	1314.26	11.42	1.88
Echinodermata	104	0	104	2.57	0.83	16115.32	517.35	2.04	0.39
Annelida	100	97	3	4.13	0.68	15473.61	958.11	2.99	0.64
Nemertea	19	0	19	6.58	0.51	15313.89	673.68	2.65	0.17
Acanthocephala	12	12	0	5	0	14123.17	524.03	8.03	0.74
Xenacoelomorpha	9	1	8	3.56	3.84	15343.33	514.44	2.73	1.43
Bryozoa	8	2	6	6.38	1.69	15390	1631.57	3.75	0.65
Hemichordata	6	0	6	1.5	0.84	16344	827.73	1.73	0.13
Brachiopoda	5	5	0	6.4	0.89	16763.2	5076.65	4.45	2
Onychophora	4	0	4	5.25	2.06	14481	685.05	2.34	0.06
Kinorhyncha	3	3	0	4.67	1.15	15091.67	183.89	5.53	0.49
Tardigrada	3	0	3	3.67	1.15	14881.33	397.31	3.69	0.23
Gnathostomulida	2	0	2	6	0	14113.5	118.09	5.56	0.09
Entoprocta	2	0	2	6	0	15092.5	325.98	2.42	0.06
Priapulida	2	0	2	4	0	14825.5	132.23	2.3	0.04
Gastrotricha	1	0	1	5		14558		3.69	0
Nematomorpha	1	0	1	5		15132		5.53	0
Orthonectida	1	0	1	8		15217		9.43	0
Phoronida	1	0	1	6		15495		2.48	0
Rotifera	1	1	0	5		15319		5.84	0

Text S3. Hypothesis 1a: Ancestral bilaterian mitogenomic architecture

We tested multiple algorithms for the ancestral gene order reconstruction in bilaterian lineages. The architecture of the ancestor of all bilaterian animals (ur-bilaterian) inferred by ProCARs algorithm produced *nad2* on the "minus" strand (by convention, the mitogenomic strand encoding a majority of genes is commonly named "plus" strand, and the opposite one "minus" strand) (Figure S1). The only other lineage for which we inferred *nad2* on the minus strand as the ancestral state was Entoprocta. This architecture also did not exhibit almost any of the commonly highly conserved bilaterian gene boxes, including the *nad4+nad4L* and *atp6+atp8* gene boxes [43]. On this basis, we rejected ProCARs results as nonsensical with high confidence.

MLGO: In combination with the "Nephrozoa" topology, this algorithm produced the architecture exhibited by most chordates, including humans ("ur-chordate" architecture henceforth) as the ur-bilaterian architecture, but with all genes encoded on the same strand, i.e. *nad6* was inverted from the minus to the plus strand (Figure S1). In more detail, the ur-chordate architecture is characterised by 12 PCGs and 2 rRNAs encoded on the "plus" strand, whereas *nad6* is encoded on the "minus" strand (opposite transcription direction), within the "*nad5 -nad6 cytb rrnS*" gene box ("-" indicates that the gene is encoded on the minus strand). MLGO produced a "*nad5 nad6 cytb rrnS*" gene box as the ancestral state for Bilateria. This gene (*nad6*) is on the minus strand in almost all Chordata, Hemichordata, Echinodermata, and Xenacoelomorpha mitogenomes, aside from a few exceptions in the latter two phyla. Given the putatively key position of Xenacoelomorpha in this topology, we suspected that it may have skewed the reconstruction. To get a better resolution, we additionally analysed all 14 annotated Xenacoelomorpha mitogenomes available in the GenBank (Figure S2). They exhibited highly scrambled gene orders, some with all genes on a single strand, so it was almost impossible to infer the ancestral position of *nad6*. When we tested the performance of MLGO in combination with the "Xenambulacraria" topology, the ancestral chordate architecture characterised by the "*nad5 -nad6 cytb*" gene box was resolved as the ancestral state for Bilateria (Figure S1). This supports our suspicions of an artefact caused by the "basal" position of Xenacoelomorpha. *Nad6* was also resolved on the minus strand in the ur-Xenambulacraria (Xenacoelomorpha+Ambulacraria) architecture, but it was translocated to the *rrnL -nad6 nad1* gene box. As regards the ur-Ambulacraria (Echinodermata+Hemichordata), it was also on the minus strand, but translocated to the *cytb -nad6 rrnS* gene box (Figure S1).

TreeREx: In combination with the "Nephrozoa" topology, this algorithm produced the ancestral chordate architecture characterised by the "*nad5 -nad6 cytb rrnS*" gene box as the ancestral state for Nephrozoa. However, *nad6* was translocated to the "*rrnS rrnL -nad6 nad1*" in the ur-bilaterian architecture (Figure S1). This gene box (*rrnL -nad6 nad1*) was not observed in the ur-chordate architecture, nor in any of the Hemichordata and Echinodermata mitogenomes. Among the six available genera for Xenacoelomorpha, it was found only in *Xenoturbella* (Figure S2). As this genus was overrepresented (6/14 mitogenomes in the dataset), we again suspected that this skewed the TreeREx reconstruction (Xenacoelomorpha was the sister-lineage to all other bilaterians in this topology). The remaining Xenacoelomorpha species exhibited highly scrambled gene orders, from which we failed to infer the ancestral arrangement of *nad6* for this phylum. When we tested the performance of TreeREx in combination with the "Xenambulacraria" topology, *nad6* was translocated between *cytb* and *rrnS* ("*nad5 cytb -nad6 rrnS*" gene box). An identical architecture was also produced

as the ancestral state for the Xenambulacraria (Xenacoelomorpha+Ambulacraria) and Ambulacraria (Echinodermata+Hemichordata) (Figure S1).

Therefore, in both cases we rejected results inferred using the Nephrozoa topology as likely to be artefactual, which leaves us with two candidates for the ancestral bilaterian architecture, both produced using the Xenambulacraria topology, and differing only in the position of *nad6*: (1) "*nad5 -nad6 cytb rrnS*" (MLGO), or (2) "*nad5 cytb -nad6 rrnS*" (TreeREx) (Figure S1).

As mitogenomic rearrangements are considered to be (nearly) a Dollo character, i.e. almost irreversible [44,45], the probability of homoplasy in mitogenomic arrangements is statistically very low. Therefore, the architecture that is found across more distantly related lineages is the most parsimonious candidate for the ancestral architecture [8,45,46]. The "*cytb -nad6*" arrangement was found only in Hemichordata, whereas the "*-nad6 cytb*" arrangement is present in most Chordata and Echinodermata. Neither arrangement was observed in Xenacoelomorpha. In addition, "*nad6 cytb*" arrangement is present in the putative ancestral architectures of both Ecdysozoa and Lophotrochozoa (Protostomia), albeit with *nad6* on the plus strand [34,42,47]. On this basis we accepted the "*-nad6 cytb*" arrangement as the most parsimonious candidate for the ancestral bilaterian mitogenome.

TreeREx_ur-Bilateria_(Nephrozoa_topology)

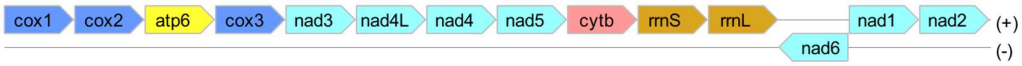

TreeREx_ur-Bilateria_(Xenambulacraria_topology)

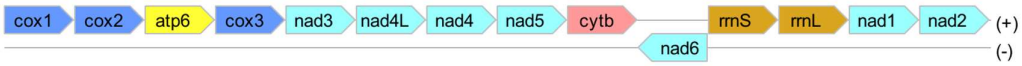

MLGO_ur-Bilateria_(Nephrozoa_topology)

MLGO_ur-Bilateria_(Xenambulacraria_topology)

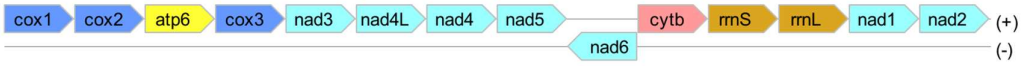

ur-Chordata_Homo_sapiens

ProCARs_ur-Bilateria_(Nephrozoa_topology)

TreeREx_ur-Nephrozoa_(Nephrozoa_topology)

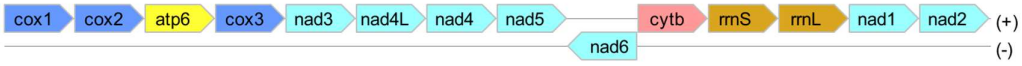

MLGO_ur-Xenambulacraria(Xenacoelomorpha+Ambulacraria)_(Xenambulacraria_topology)

TreeREx_ur-Xenambulacraria(Xenacoelomorpha+Ambulacraria)_(Xenambulacraria_topology)

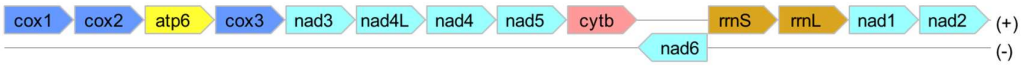

MLGO_ur-Ambulacraria(Hemichordata+Echinodermata)_(Xenambulacraria_topology)

TreeREx_ur-Ambulacraria(Hemichordata+Echinodermata)_(Xenambulacraria_topology)

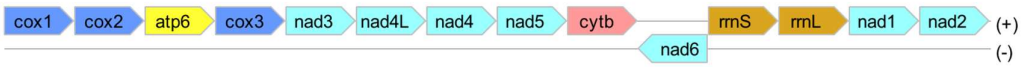

TreeREx_ur-Ambulacraria(Hemichordata+Echinodermata)_(Nephrozoa_topology)

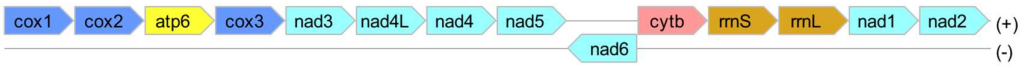

TreeREx_ur-Protostomia_(Nephrozoa_topology)

TreeREx_ur-Ecdysozoa_(Nephrozoa_topology)

Figure S1. Candidates for ancestral mitogenomic architectures of major bilaterian lineages produced across different algorithms (TreeREx, MLGO, ProCARs) and topologies (Nephrozoa and Xenambulacraria). Prefix "ur" stands for ancestral; (+) and (-) indicate mitogenomic "plus" and "minus" strands respectively; *atp8* was removed from all TreeREx analyses (missing genes not allowed), and removed from all ur-Bilateria candidates to facilitate visual comparisons (its ancestral position upstream from *atp6* is firmly confirmed).

Figure S2. All available Xenacoelomorpha mitogenomes and their architectures. (+) and (-) indicate mitogenomic "plus" and "minus" strands respectively.

Text S4. Hypothesis 1b: Evolutionary history of strand distribution of genes

Aside from Bilateria, our analyses also produced double-stranded architecture as the ancestral state for Deuterostomia (or Xenambulacraria in alternative topologies), Protostomia, and both superphyla forming the latter clade: Ecdysozoa and Lophotrochozoa (Figure S1).

Chordata

All Tunicata (subphylum) included in the main dataset exhibited a single-stranded architecture, which is a recognised feature [48], but all belonged to the class Ascidiacea. To get a better resolution, we retrieved all 122 Tunicata mitogenomes from the GenBank. Among these 122 mitogenomes, 7 mitogenomes belonged to the class Thaliacea, 3 to Appendicularia, and all other belonged to Ascidiacea. Ascidiacea and Thaliacea consistently exhibited single-stranded architectures. In contrast, among the Appendicularia, all three species belonged to the genus *Oikopleura*: one was single-stranded (*O. sp. bigama* LC830956), and two mitogenomes were double-stranded - *O. dioica* (OZ035851) and *Oikopleura* sp. (PP146516) (Figure S3). The mitogenome of *Oikopleura dioica* has been sequenced, and its unique features discussed, multiple times [49–52]. Among these, only two studies observed that genes are encoded on both strands [51,52], but did not further discuss the relevance of this observation. There are some indications that Appendicularia may be the sister clade to all other tunicates [53], which indicates that this class may exhibit the ancestral double-stranded architecture, but the single-stranded architecture of *O. sp. bigama* (LC830956) [54] contradicts this proposal. Notably, the annotation of appendicularian mitogenomes is extremely difficult, with rapidly-evolving, highly divergent genes, in addition to the incomplete gene set, hampering the annotation [51,52]. In this light, the first scenario we should consider is that this is an annotation artefact, and the possibility that this species actually does have genes encoded on the minus strand. Assuming that the annotation is correct, there are multiple scenarios: (1) double-strand is the ancestral state for Appendicularia, so there is a second independent double-single transition in some *Oikopleura* species; (2) single-strand is the ancestral state for all Tunicata, and some *O. dioica* that mitogenomes underwent a single-double transition (state-reversal). Mitogenomes for more Appendicularia species and lineages should be sequenced and annotated in order to be able to answer this question.

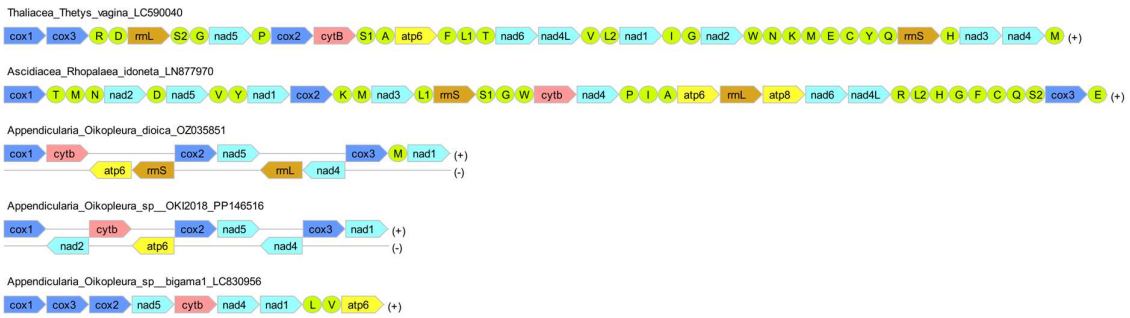

Figure S3. Selected Tunicata mitogenomic architectures. (+) and (-) indicate mitogenomic "plus" and "minus" strands respectively. Class is shown before the species name.

Ecdysozoa

The identified ancestral PCGs+rRNAs arrangement for Ecdysozoa was found in 3068 out of 3476 Arthropoda species, 2 out of 3 Tardigrada, and 1 out of 4 Onychophora. Phyla exhibiting exclusively double-stranded mitogenomic architectures were: Priapulida (2/2 species), Tardigrada (2/2 species), Nematomorpha (1/1 species), Onychophora (4/4 species). Phyla exhibiting exclusively single-stranded mitogenomic architectures: Kinorhyncha: (3/3 species). A putative double-to-single switch was inferred in the common ancestor of Kinorhyncha (Figure S4), because the sister clade, Priapulida, exhibits a double-stranded state.

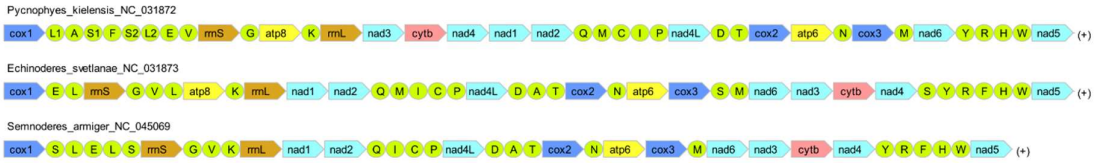

Figure S4. Mitogenomic architectures of all three available Kinorhyncha species.

Nematoda: 148 single-stranded, and 26 double-stranded mitogenomes in the RefSeq dataset. Within this phylum, the class Enoplea consistently double-stranded (26/26), and the class Chromadorea consistently single-stranded (148/148). A single transition is inferred in the common ancestor of Chromadorea.

Arthropoda: 4 species had single-stranded, and 3500 had double-stranded mitogenomes. Both available Polydesmida (Arthropoda; Myriapoda; Diplopoda; Helminthomorpha; Polydesmida) mitogenomes included in the original dataset had all genes on a single strand, so we downloaded all available mitogenomes from GenBank, and confirmed that all seven were single-stranded (Figure S5). The uniqueness of single-stranded architecture of this clade had not been recognised before apparently, e.g. [55], but the inversion of half of the mitochondrial genome in *Appalachioria falcifera* (NC_021933) has been recognised as a major rearrangement, unprecedented in myriapods [56].

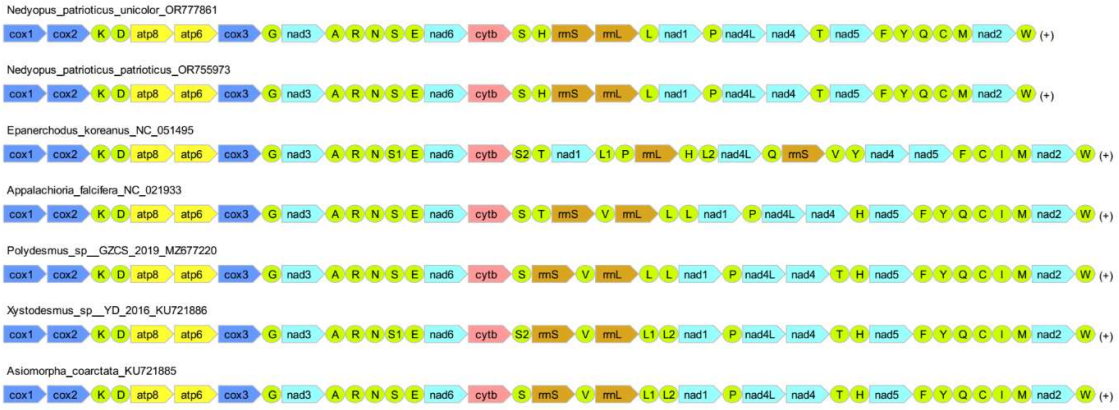

Figure S5. Mitogenomic architectures of seven available Polydesmida species.

Two independent state shifts were observed in Copepoda (Arthropoda; Crustacea; Multicrustacea; Hexanauplia): one in the order Calanoida and the other in Harpacticoida. (1) Among the three mitogenomes of species belonging to the order Calanoida, one species had all genes on a single strand: *Eurytemora affinis* (NC_046694; family Temoridae). To get a better resolution, we downloaded all 32 available mitogenomes from GenBank, and identified only one more single-stranded architecture: *Labidocera rotunda* (Pontellidae) (Figure S6). As Temoridae and Pontellidae are sister families [57], and these were the only representatives of these families, we inferred a double-to-single transition in a common ancestor of Temoridae+Pontellidae as the most parsimonious scenario. The authors that sequenced the mitogenome *E. affinis* did not observe that is it unique in its distribution of genes; they merely observed that it resembles *Tigriopus* [58]. (2) Among the Harpacticoida, Harpacticidae, one *Tigriopus* species exhibited a single-stranded architecture: *Tigriopus californicus* in the original dataset. This unique architecture, along with extremely high levels of divergence, was observed in the associated study [59]. We retrieved all Copepoda mitogenomes, and confirmed the single-stranded architecture on all four available *T. californicus* mitogenomes, as well as two *Tigriopus japonicus* mitogenomes. However, the third available *Tigriopus* species, *Tigriopus kingsejongensis*, had genes encoded on both strands, and its sequence was highly divergent compared to the former two species (Figure S7).

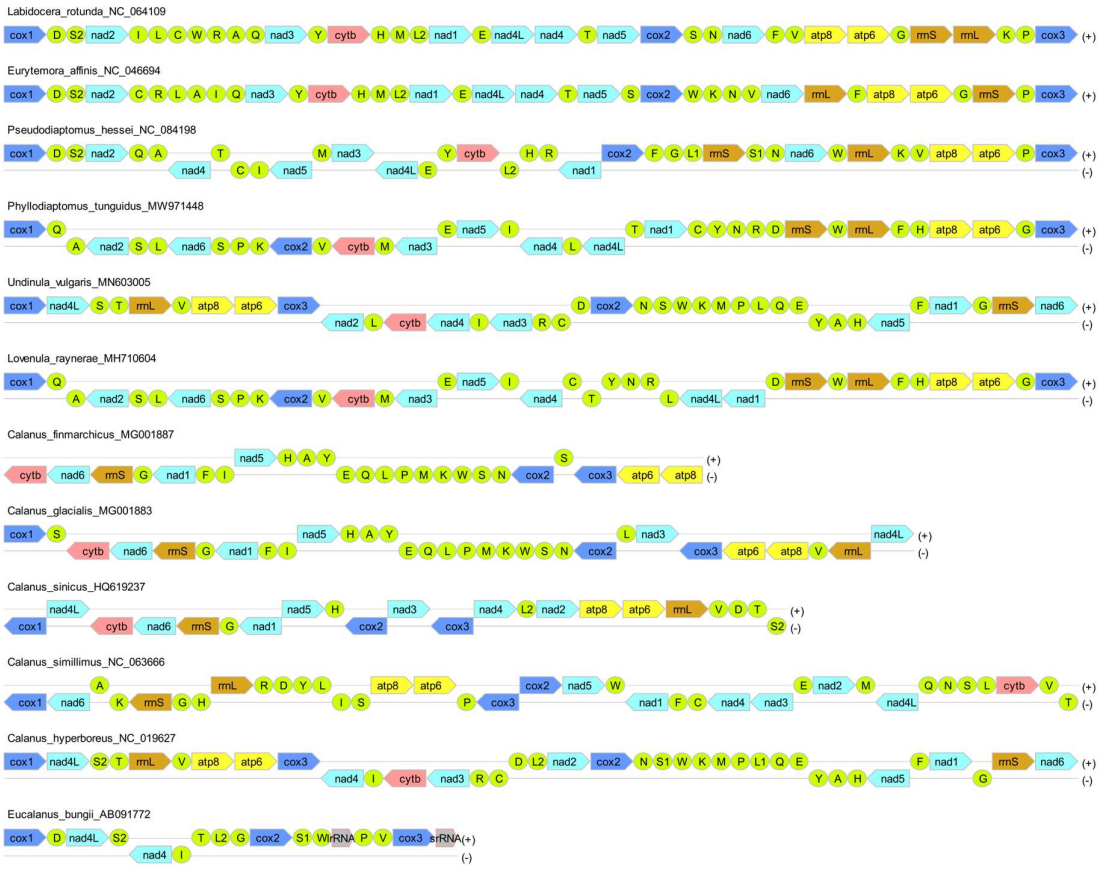

Figure S6. Mitogenomic architectures of Calanoida (one mitogenome per species selected for visualisation).

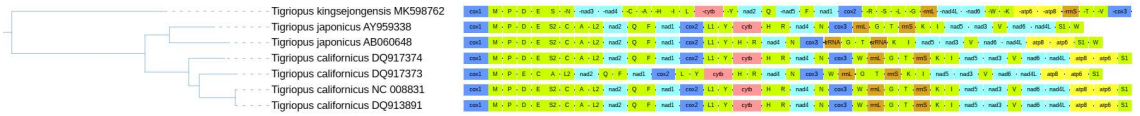

Figure S7. Mitogenomic architectures of all seven available *Tigriopus* species, with phylogeny inferred using concatenated mitochondrial PCGs.

Lophotrochozoa

Overall, Lophotrochozoa was the most "problematic" lineage due to highly rearranged mitogenomic architectures, often exhibiting few or no plesiomorphies with the ur-bilaterian architecture. We tested the performance of different datasets and algorithms, but likely due to the highly rearranged mitogenomic architectures of most lineages, we failed to reconstruct of the ancestral architecture for this superphylum with confidence (Figure S8). However, multiple lines of evidence strongly support double-stranded arrangement as the ancestral one, including most of our own results.

To reduce the amount of noise, we reduced the dataset to only a few species per phylum, either comprising only species exhibiting gene orders conserved across multiple phyla, or belonging to "basal" (early-diverging) lineages. Starting with the putative ancestral double-stranded architecture for Protostomia (Figure S1), the scenario of single-strand as the ancestral state for Lophotrochozoa requires a shift of two gene blocks from minus strand to plus strand: *nad5-nad4-nad4L* and *nad1-rrnL-rrnS*. This would then require multiple single-strand-to-double-strand shifts in the common ancestors of major lophotrochozoan lineages (Gnathifera, Gastrotricha+Platyhelminthes, and the common ancestor of remaining phyla; note that the topology of this clade is unresolved, so the scenario may differ depending on the topology). The hypothesis of double-stranded ancestral lophotrochozoan requires a much simpler, and therefore much more parsimonious scenario.

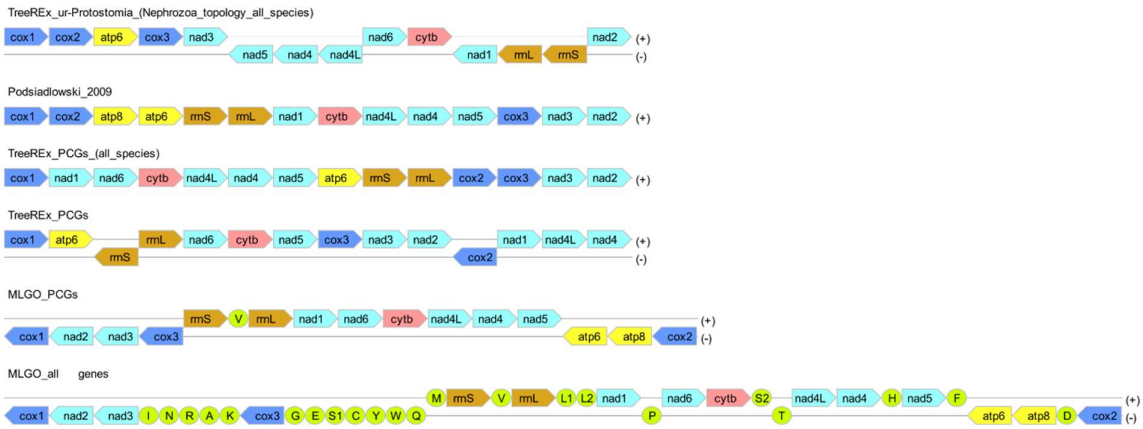

Figure S8. Candidates for ancestral mitogenomic architectures of Lophotrochozoa produced across different algorithms (TreeREx, MLGO) and datasets. "All species" in the name indicates that all Lophotrochozoa mitogenomes in the dataset we included in the dataset. For others, only a few selected species (basal lineages or putatively ancestral architectures) were used per phylum. tRNAs were included in one dataset ("all genes"), and excluded from other datasets (only PCGs+rRNAs included). Prefix "ur" stands for "ancestral". (+) and (-) indicate mitogenomic "plus" and "minus" strands respectively. *atp8* was removed from all TreeREx analyses (missing genes not allowed). "Podsiadlowski_2009" is the ur-Lophotrochozoa architecture proposed by Podsiadlowski et al. [42].

Previous studies proposed the architecture found in several Nemertea species as the ancestral lophotrochozoan architecture on the basis of its similarity with the ancestral architecture for Mollusca and Phoronida [42,47,60,61]. Whereas Mollusca and Nemertea are likely to be sister phyla, Phoronida is more distantly related [62]. In the ancestral Nemertea architecture, only *trnT* and *trnP* are encoded on the minus strand (Figure S9). Indeed, a similar, architecture, is also shared by Entoprocta albeit inverted. However, this group of phyla forms Platyzoa or Lophotrochozoa sensu stricto, and comparison with other phyla does not indicate that it can be considered ancestral for the remaining lophotrochozoan phyla. In more detail, there is some discrepancy in the definition of Lophotrochozoa between different scientists, and the relationships within the clade remain unresolved [63,64]. Herein we use Lophotrochozoa sensu lato definition, comprising a monophyletic sister-superphylum to Ecdysozoa, and we accounted for this discrepancy in definitions in the interpretation of previous findings.

The ancestral bilaterian "*cox1 cox2 atp8 atp6*" box (Figure S1) was observed in multiple phyla (Nemertea, Mollusca, Annelida) (Figure S9), so we can safely assume that it was present in the ur-Lophotrochozoa. Previous studies proposed that this was followed by the "*rrnS rrnL nad1*" box in the ur-lophotrochozoan architecture, also conserved in other bilaterian lineages [42,47]. This box was found in the proposed position, downstream from the "*cox1…atp6*" box, only in Nemertea. We observed it in a few other phyla, but in different locations: in Annelida (*Magelona mirabilis*) it has been transposed, whereas in Mollusca (*Katharina tunicata*) and Phoronida it has been inverted and transposed (minus strand). Notably, the "*rrnS rrnL*" box was conserved across most phyla, but its position varied. In the proposed ur-lophotrochozoan architecture, the downstream gene box comprises another highly conserved bilaterian box, "*nad6 cytb*", already discussed herein (Text S3). In the proposed ancestral position, it was found only in Nemertea. In Mollusca, the location was downstream from the "*rrnS rrnL nad1*" box, as the entire section underwent an inversion. It was also found in Gnathostomulida (transposed), Entoprocta, Bryozoa Phoronida, Annelida, Orthonectida (all transposed-inverted). Further downstream in the proposed ur-lophotrochozoan architecture is another conserved bilaterian box: "*nad4L nad4 nad5*". It was observed only in several phyla, but translocated in all cases. In Entoprocta, it was transposed-inverted together with the upstream "*nad1 nad6 cytb*" box. In Mollusca and Phoronida, it was transposed-inverted together with the upstream "*rrnS rrnL nad1 nad6 cytb*" box. In Bryozoa (*Pectinatella magnifica*), also transposed-inverted - together with the upstream "*nad1 nad6 cytb*" box (rearranged architecture otherwise). The next downstream bilaterian box, *cox3-nad3* was found in multiple phyla: Gnathostomulida (transposed), Entoprocta (transposed-inverted together with the upstream *nad1-nad6-cytb* box), Mollusca and Phoronida (inverted together with the upstream *rrnS-rrnL-nad1-nad6-cytb* box), Bryozoa (*Pectinatella magnifica*) - together with the

upstream *nad1-nad6-cytb* box (rearranged architecture otherwise), and Annelida (*nad6-cytb* transposed elsewhere, otherwise conserved) (Figure S9).

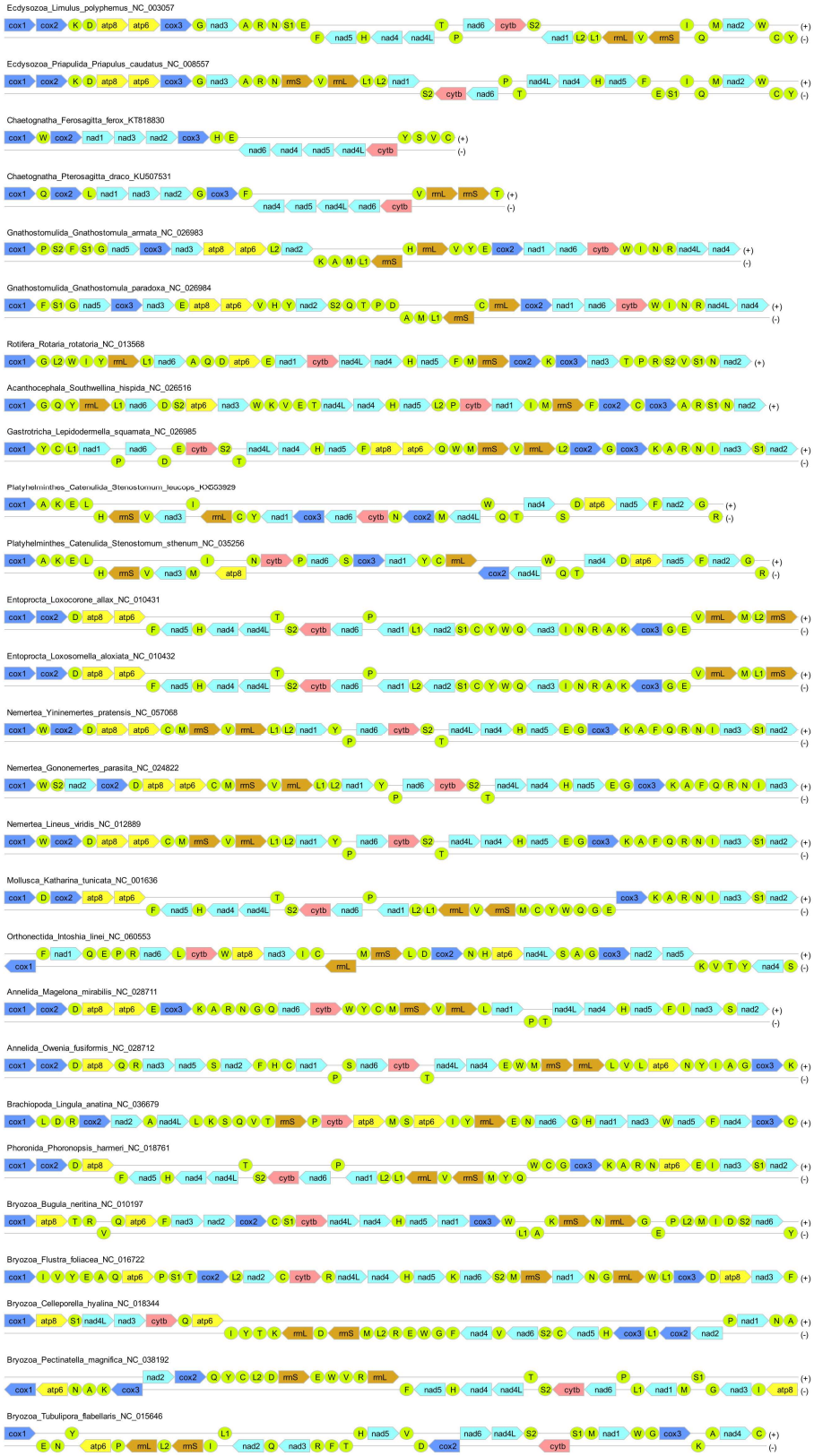
Ecdysozoa_Limulus_polyphemus_NC_003057
Ecdysozoa_Priapulida_Priapulus_caudatus_NC_008557
Chaetognatha_Ferosagitta_ferox_KT818830
Chaetognatha_Pterosagitta_draco_KU507531
Gnathostomulida_Gnathostomula_armata_NC_026983
Gnathostomulida_Gnathostomula_paradoxa_NC_026984
Rotifera_Rotaria_rotatoria_NC_013568
Acanthocephala_Southwellina_hispida_NC_026516
Gastrotricha_Lepidodermella_squamata_NC_026985
Platyhelminthes_Catenulida_Stenostomum_leucops_KX553929
Platyhelminthes_Catenulida_Stenostomum_sthenum_NC_035256
Entoprocta_Loxocorone_allax_NC_010431
Entoprocta_Loxosomella_aloxiata_NC_010432
Nemertea_Yininemertes_pratensis_NC_057068
Nemertea_Gononemertes_parasita_NC_024822
Nemertea_Lineus_viridis_NC_012889
Mollusca_Katharina_tunicata_NC_001636
Orthonectida_Intoshia_linei_NC_060553
Annelida_Magelona_mirabilis_NC_028711
Annelida_Owenia_fusiformis_NC_028712
Brachiopoda_Lingula_anatina_NC_036679
Phoronida_Phoronopsis_harmeri_NC_018761
Bryozoa_Bugula_neritina_NC_010197
Bryozoa_Flustra_foliacea_NC_016722
Bryozoa_Celleporella_hyalina_NC_018344
Bryozoa_Pectinatella_magnifica_NC_038192
Bryozoa_Tubulipora_flabellaris_NC_015646

Figure S9. Mitogenomic architectures of selected representatives of lophotrochozoan phyla. The phylum name is followed by the species name and GenBank accession number. tRNA genes are included. (+) and (-) indicate mitogenomic "plus" and "minus" strands respectively. Two ecdysozoan species exhibiting conserved ancestral architectures are shown at the top.

Brachiopoda: All available species exhibited a single-stranded architecture (Figure S10). Double-to-single transition in the common ancestor of the entire phylum is the most parsimonious scenario given the currently available dataset.

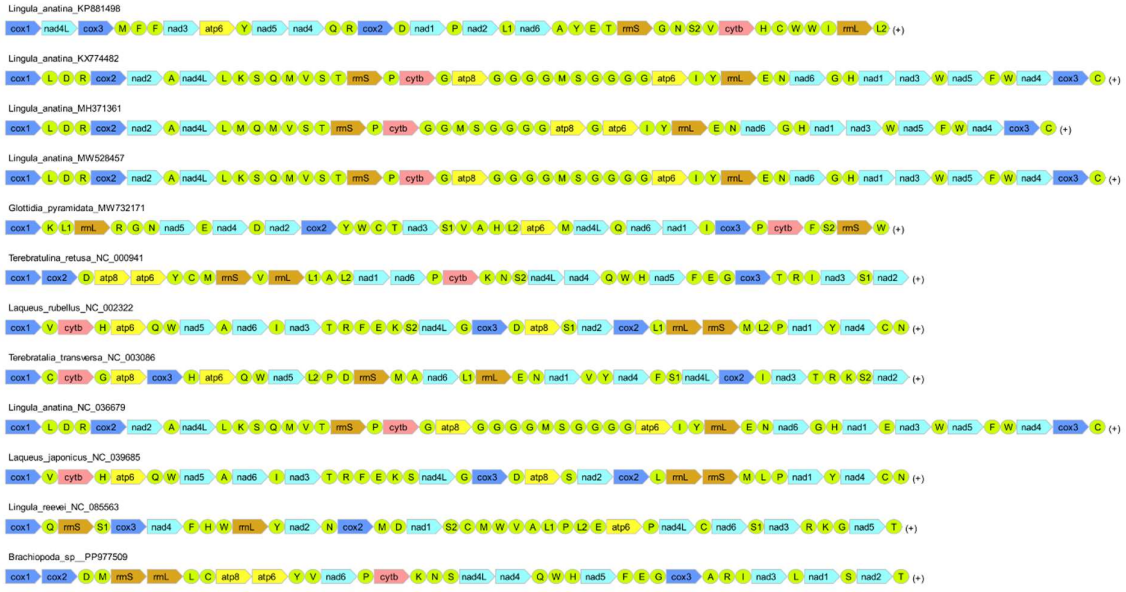

Figure S10. Mitogenomic architectures of all available Brachiopoda species.

Gnathifera: Within the clade Gnathifera, the single-stranded architectural type is limited to the derived [62] Syndermata (Rotifera+Acanthocephala) (Figures S11-S12), whereas Chaetognatha and Gnathostomulida both have double-stranded ancestral architectures (Figure S9). On this basis, double-strand architecture is the parsimonious ancestral state for Gnathifera, as it requires only one double-to-single shift in the ancestor of Syndermata. In contrast, the alternative scenario would require single-to-double shifts in these two phyla, which are evolutionarily rare and not observed with confidence outside Mollusca and Annelida. In Rotifera, which predominantly exhibit fragmented mitogenomes, we observed three species that exhibited a combination of single-stranded and double-stranded architectures (Figure S12). Due to the fragmentation of their genomes, these could easily be annotation artefacts.

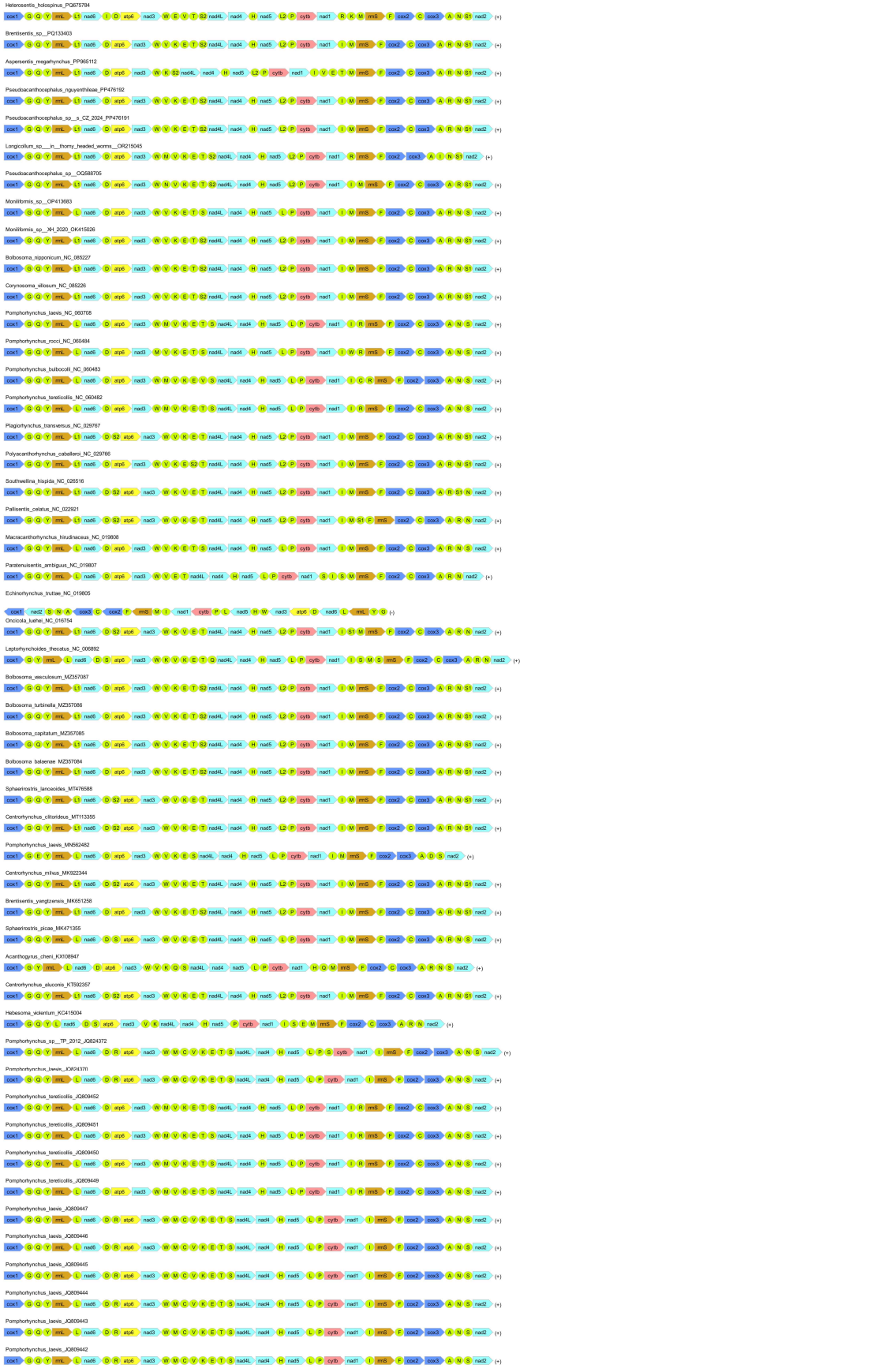
Heterosentis_holospinus_PQ675784
Brentisentis_sp__PQ133403
Aspersentis_megarhynchus_PP965112
Pseudoacanthocephalus_nguyenthileae_PP476192
Pseudoacanthocephalus_sp__s_CZ_2024_PP476191
Longicollum_sp___in__thomy_headed_worms__OR215045
Pseudoacanthocephalus_sp__OQ588705
Moniliformis_sp__OP413683
Moniliformis_sp__XH_2020_OK415026
Bolbosoma_nipponicum_NC_085227
Corynosoma_villosum_NC_085226
Pomphorhynchus_laevis_NC_060708
Pomphorhynchus_rocci_NC_060484
Pomphorhynchus_bulbocolli_NC_060483
Pomphorhynchus_tereticollis_NC_060482
Plagiorhynchus_transversus_NC_029767
Polyacanthorhynchus_caballeroi_NC_029766
Southwellina_hispida_NC_026516
Pallisentis_celatus_NC_022921
Macracanthorhynchus_hirudinaceus_NC_019808
Paratenuisentis_ambiguus_NC_019807
Echinorhynchus_truttae_NC_019805
Oncicola_luehei_NC_016754
Leptorhynchoides_thecatus_NC_006892
Bolbosoma_vasculosum_MZ357087
Bolbosoma_turbinella_MZ357086
Bolbosoma_capitatum_MZ357085
Bolbosoma_balaenae_MZ357084
Sphaerirostris_lanceoides_MT476588
Centrorhynchus_clitoridesus_MT113355
Pomphorhynchus_laevis_MN562482
Centrorhynchus_milvus_MK922344
Brentisentis_yangtzensis_MK851258
Sphaerirostris_picae_MK471355
Acanthogyrus_cheni_KX108947
Centrorhynchus_aluconis_KT592357
Hebesoma_violentum_KC415004
Pomphorhynchus_sp__TP_2012_JQ824372
Pomphorhynchus_laevis_JQ809447
Pomphorhynchus_laevis_JQ809446
Pomphorhynchus_laevis_JQ809445
Pomphorhynchus_laevis_JQ809444
Pomphorhynchus_laevis_JQ809443
Pomphorhynchus_laevis_JQ809442

Figure S11. Mitogenomic architectures of most available Acanthocephala.

Figure S12. Mitogenomic architectures of most available Rotifera.

Platyhelminthes: Despite the vast majority of Platyhelminthes exhibiting a single-stranded architecture, we inferred a double-stranded ancestral architecture for this phylum, because both

available mitogenomes in the "basal" radiation (i.e. sister clade to all other Platyhelminthes), Catenulida [65,66], exhibited a double-stranded architecture [67] (Figure S13). In this scenario, only one double-to-single transition is required in the common ancestor of the remaining Platyhelminthes ("turbellaria+Neodermata", all single-stranded), whereas two transitions would be required assuming single-stranded as the ancestral state for the entire phylum. The putative sister-phylum, Gastrotricha, exhibits a double-stranded architecture, albeit only with three tRNA genes on the minus strand (Figure S9). This implies that the most likely ancestral state for Platyhelminthes is double-stranded.

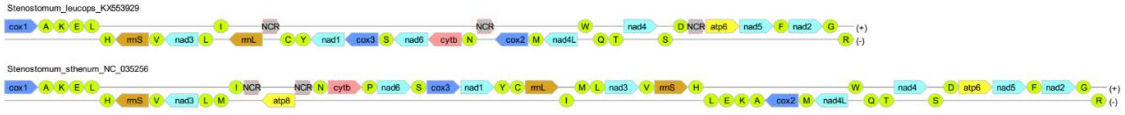

Figure S13. Mitogenomic architectures of both available Catenulida species.

Entoprocta: Exhibited a large number of genes on the minus strand (Figure S9). The most likely ancestral state is double-stranded.

Phoronida: Only one species was available, with multiple genes on the minus strand (*Phoronopsis harmeri*; NC_018761; Figure S9). Double-stranded ancestral architecture is the most parsimonious scenario given the currently available dataset.

Bryozoa: *Pectinatella magnifica* (Pectinatellidae) from the "basal" radiation Phylactolaemata [68] exhibited a double-stranded architecture (Figure S14). On this basis, we inferred double-stranded as the ancestral state, and putatively three derived double-to-single evolutionary shifts: (1) Flustridae+Antroporidae sister families [68]; (2) *Watersipora subtorquata* (putatively all Watersiporidae); (3) *Exechonella vieirai* (putatively all Exechonellidae). Due to the unresolved phylogeny of Bryozoa [68] and poor lineage coverage, the evolutionary history of transitions in this phylum is likely to be partial.

Figure S14. Mitogenomic architectures of all available Bryozoa species.

Nemertea: This phylum putatively forms a sister clade with highly variable and unique Mollusca. We additionally extracted all 44 Nemertea mitogenomes available in the GenBank. They exhibited a remarkably conserved architecture, with almost all genes on the plus strand, apart from *trnP* and *trnT* (Figure S15).

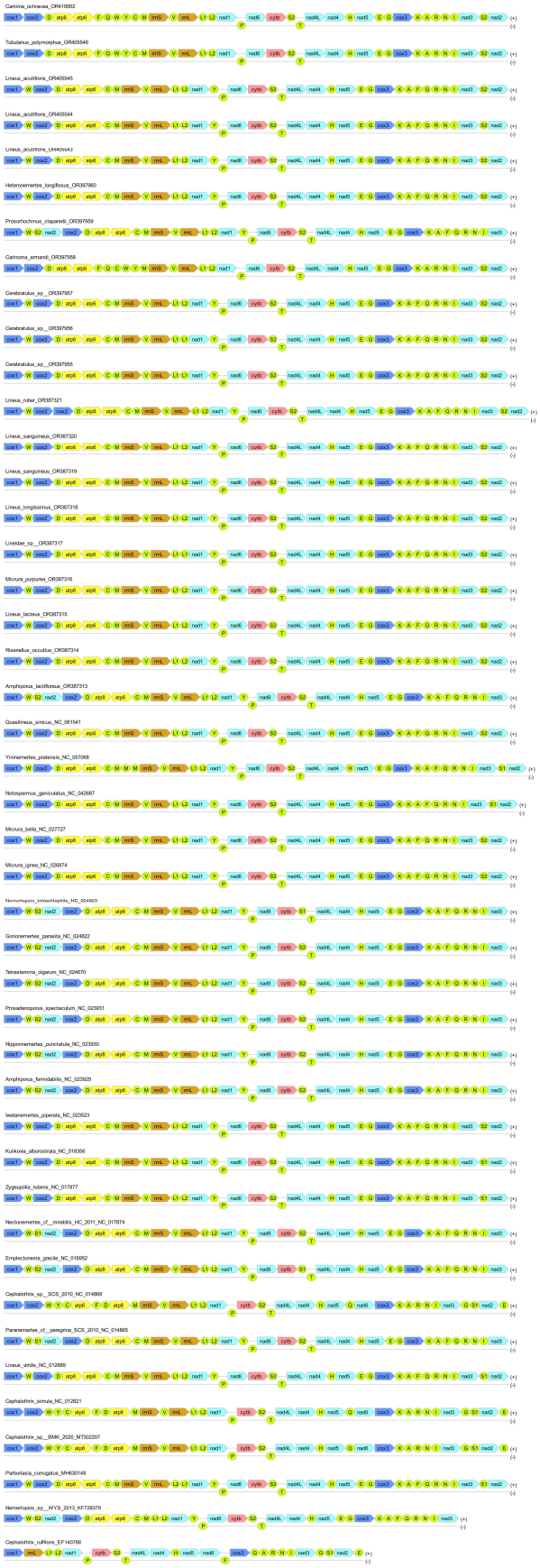
Carinina_ochracea_OR419932
Tubulanus_polymorphus_OR405546
Lineus_acutifrons_OR405545
Lineus_acutifrons_OR405544
Lineus_acutifrons_LR491643
Heteronemertes_longifissus_OR397960
Prosorhochmus_claparedii_OR397959
Carinoma_armandi_OR397958
Cerebratulus_sp__OR397957
Cerebratulus_sp__OR397956
Cerebratulus_sp__OR397955
Lineus_ruber_OR387321
Lineus_sanguineus_OR387320
Lineus_sanguineus_OR387319
Lineus_longissimus_OR387318
Lineidae_sp__OR387317
Micrura_purpurea_OR387316
Lineus_lacteus_OR387315
Riseriellus_occultus_OR387314
Amphiporus_lactifloreus_OR387313
Quasilineus_sinicus_NC_061541
Yininemertes_pratensis_NC_057066
Notospermus_geniculatus_NC_042667
Micrura_bella_NC_027727
Micrura_ignea_NC_029874
Nemertopsis_tohnoiikkaihka_NC_024920
Gononemertes_parasita_NC_024822
Tetrastemma_olgarum_NC_024670
Prosadenoporus_spectaculum_NC_023931
Nippenemertes_punctatula_NC_023930
Amphiporus_formidabilis_NC_023929
Iwatanemertes_piperata_NC_023523
Kulikovia_alborostrata_NC_018356
Zygeupolia_rubens_NC_017877
Nectonemertes_cf__mirabilis_HC_2011_NC_017874
Emplectonema_gracile_NC_016952
Cephalothrix_sp__SCS_2010_NC_014899
Paranemertes_cf__peregrina_SCS_2010_NC_014865
Lineus_viridis_NC_012889
Cephalothrix_simula_NC_012821
Cephalothrix_sp__BMK_2020_MT592207
Parborlasia_corrugatus_MH630149
Nemertopsis_sp__WYS_2013_KF728379
Cephalothrix_rufifrons_EF140788

Figure S15. Mitogenomic architectures of all available Nemertea.

Annelida:

A single-stranded architecture was exhibited by most species of Errantia and Sedentaria, the two major annelid groups [45]. However, while it is likely that this is the ancestral gene order for these two major clades, Oweniidae and Magelonidae form a monophyletic group Palaeoannelida, which constitutes the sister taxon of the remaining annelids [69]. These two species both exhibit double-stranded architecture, but only with two tRNA genes encoded on the minus strand (Figure S9), which may be an indication of an evolutionary step towards a single-stranded architecture. The architecture observed in the putative sister-phylum Orthonectida [62,70] was double-stranded, with a highly rearranged architecture (Figure S9). However, it comprised a block of genes found only in *Owenia fusiformis* (Figure S9) among the three annelid candidates (*Magelona mirabilis* and the ancestral Errantia and Sedentaria architecture). On this basis, we propose that the architecture of *Owenia fusiformis* might be the most similar to the ancestral architecture of Annelida. This was followed by a shift to the single-strand state in all other Annelida (Errantia and Sedentaria). Among these, a single Sedentaria species, *Sabella spalanzani* (Sabellidae), exhibited a double-stranded architecture. Its unique architecture was observed in the original study [71]. Three annotated mitogenomes belonging to this species are available in GenBank, from two teams, and all three exhibit the identical double-stranded architecture (Figure S16). Only one annotated mitogenome belonging to another species from the same family (Sabellidae) was found, *Pseudopotamilla reniformis*, but this mitogenome exhibits a standard annelid single-stranded architecture. Remarkably, *S. spalanzani* had 19 genes on the minus strand (confirmed on three specimens), requiring multiple strand inversions in comparison to *P. reniformis* (Figure S16). As this family is derived within the Annelida [69], this is the first confirmed single-stranded to double-stranded evolutionary transition.

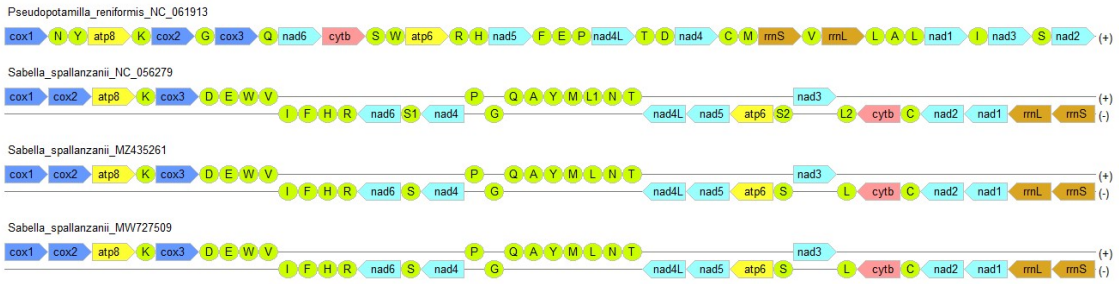

Figure S16. Mitogenomic architectures of all available Sabellidae species.

Mollusca (Figures S17-S38): In Mollusca, the most likely ancestral architectural type is also double-stranded, as early-diverging lineages, comprising Aplacophora, Polyplacophora, Monoplacophora, and Cephalopoda [72,73], all exhibit double-stranded architectures [60,74,75]. TreeREx reconstruction also produced an ancestral double-stranded architecture, and BayesTraits also inferred double-stranded with 99.999 probability. State shifts were observed only in two major derived clades: Gastropoda and Bivalvia.

Gastropoda: Most species had genes on both strands, but outliers were observed in two lineages. In Patellogastropoda, the basal gastropod lineage, most species had the ancestral molluscan double-stranded architecture. This implies that double-stranded is the ancestral state for Gastropoda. The outlier in Patellogastropoda was *Scurria scurria* (Lottioidea: Acmaeidae or Lottiidae, taxonomic incongruence), which exhibited a single-stranded architecture. All other Lottioidea mitogenomes were double-stranded. The authors of this mitogenome annotated all genes on the minus strand, so we suspect an annotation artefact.

There were also several single-stranded mitogenomes in the superfamily Buccinoidea (Caenogastropoda: Neogastropoda). The ancestral architecture for this superfamily is double-stranded (observed in a vast majority of mitogenomes), and gene order is perfectly conserved across all species (disregarding likely annotation artefacts and strand switches). In the ancestral architecture, *trnT* and a large tRNA gene box *MYCWQGE* are on the minus strand (Figures S17 – S27). However, multiple isolated species exhibited all genes on the plus strand (with unchanged gene orders – just the 8 tRNA genes switched to the plus strand). In the family Tudiclidae (taxonomic discrepancy: Buccinidae in GenBank), single-stranded architectures were observed in two genera: (1) within the genus *Aeneator*, three out of five species exhibited single-stranded architectures: *benthicolus*, *otagonensis* and *valedictus* (*A. elegans* and *recens* exhibited double-stranded architectures; Figure S17); (2) within the genus *Buccinulum*, three out of five species were also single-stranded (Figure S18).

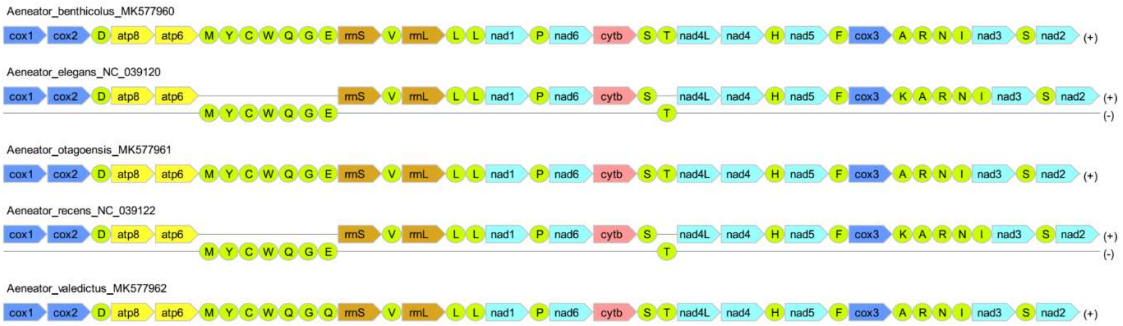

Figure S17. Mitogenomic architectures of all available *Aeneator* sp. (Tudiclidae; taxonomic discrepancy: Buccinidae in GenBank) GenBank entries.

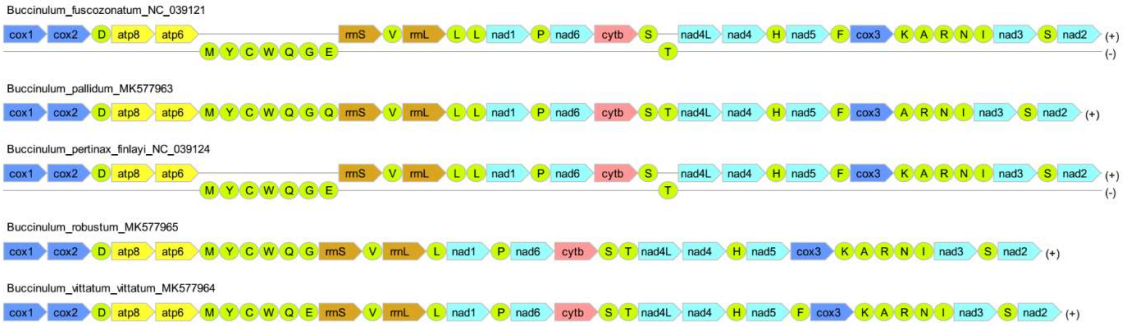

Figure S18. Mitogenomic architectures of all available *Buccinulum* (Tudiclidae; taxonomic discrepancy: Buccinidae in GenBank) GenBank entries.

In the family Babyloniidae (taxonomic discrepancy: Buccinidae in GenBank), one out of four *Babylonia* species was single-stranded: *Babylonia bomeensis* (Figure S19).

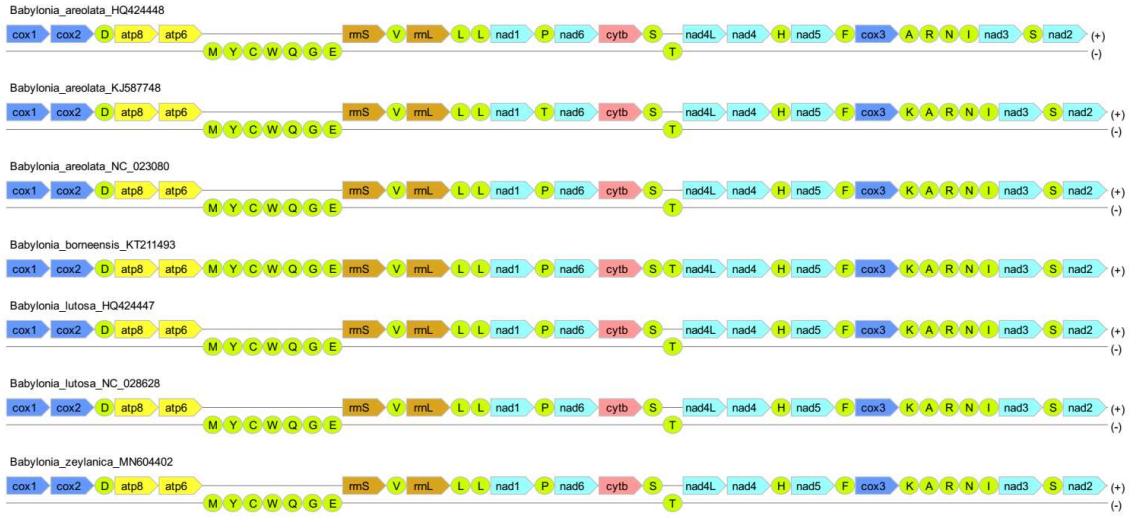

Figure S19. Mitogenomic architectures of all available *Babylonia* (Babyloniidae; taxonomic discrepancy: Buccinidae in GenBank) GenBank entries.

In the family Buccinidae single-stranded architectures were observed in three genera: (1) within the genus *Buccinum*, two out of five species were single-stranded (Figure S20); and the only representatives of the genera (2) *Volutopsius* (*norwegicus*) (Figure S21), and (3) *Pararetifusus* (*carinatus*) were single-stranded (Figure S22). In the family Colidae, the only representative of the genus *Colus* (*islandicus*) was single-stranded (Figure S22).

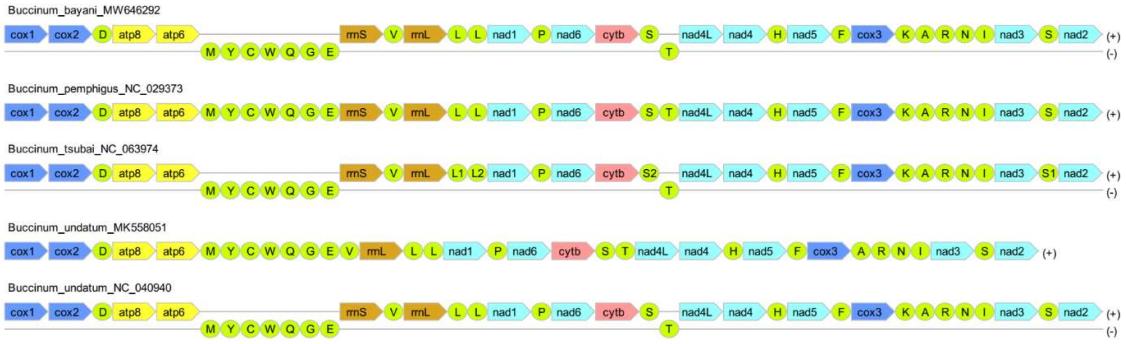

Figure S20. Mitogenomic architectures of all available *Buccinum* (Buccinidae) GenBank entries.

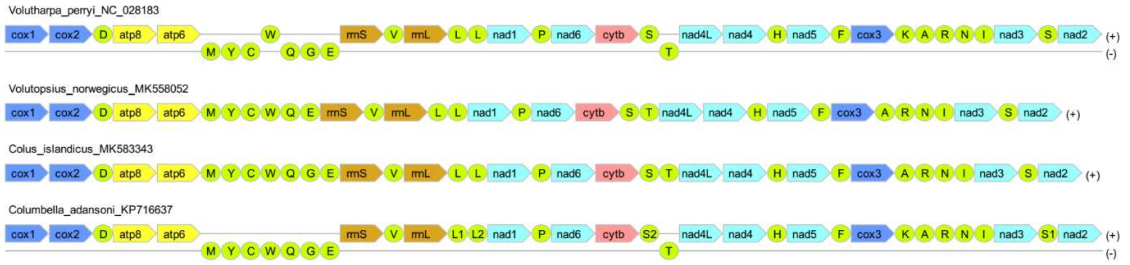

Figure S21. Mitogenomic architectures of all available *Volutopsius* (Buccinidae) and *Colus* (Colidae) GenBank entries.

Figure S22. Mitogenomic architecture of the only available *Pararetifusus* (Buccinidae) GenBank entry.

In the family Fasciolariidae, single-stranded architectures were observed in two genera: (1) the only available *Glaphyrina* (*G. caudata*) and *Taron* species (*T. dubius*) were single-stranded (Figures S23 and S24 respectively).

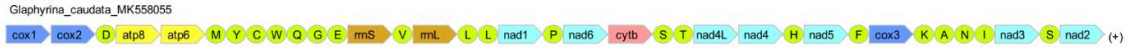

Figure S23. Mitogenomic architecture of the only available *Glaphyrina* (Fasciolariidae) GenBank entry.

Figure S24. Mitogenomic architecture of the only available *Taron* (Fasciolariidae) GenBank entry.

In the family Cominellidae, one out of two *Cominella* species was single-stranded (Figure S25).

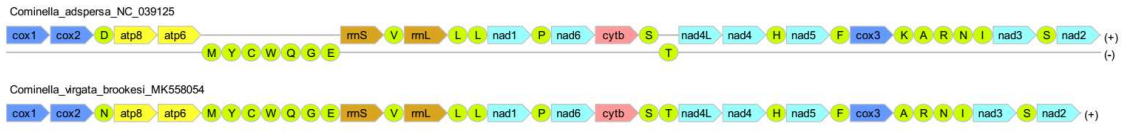

Figure S25. Mitogenomic architectures of both available *Cominella* (Cominellidae) GenBank entries.

In the family Austrosiphonidae, two out of seven *Penion* species were single-stranded (Figure S26).

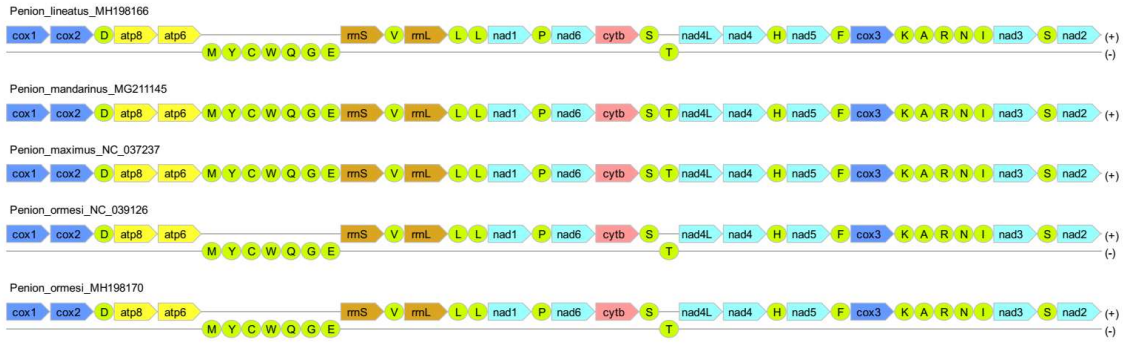

Figure S26. Mitogenomic architectures of a selection of *Penion* (Austrosiphonidae) GenBank entries, showing the two single-stranded architectures.

In the family Prosiphonidae, the only representative of the genus *Austrofusus* was single-stranded: *Austrofusus glans* (Figure S27).

Figure S27. Mitogenomic architecture of the only available *Austrofusus* (Prosiphonidae) GenBank entry.

In the family Nassariidae, single-stranded architectures were observed in two out of five species from the genus *Nassarius*: *granifer* and *hepaticus* (Figure S28).

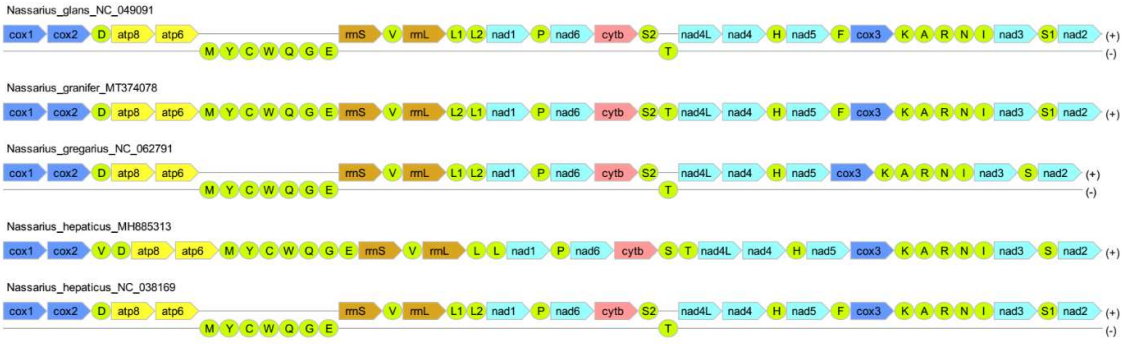

Figure S28. Mitogenomic architectures of all *Nassarius* (Nassariidae) GenBank entries.

In addition, *Scurria scurria* of the family Acmaeidae (Patellogastropoda: Lottioidea; WormBase lists it as Lottiidae) exhibited a single-stranded architecture (Figure S29). The authors annotated all genes on the minus strand, so we suspect a possibility of an annotation artefact. All other Lottioidea mitogenomes were double-stranded. An annotation artefact is likely here.

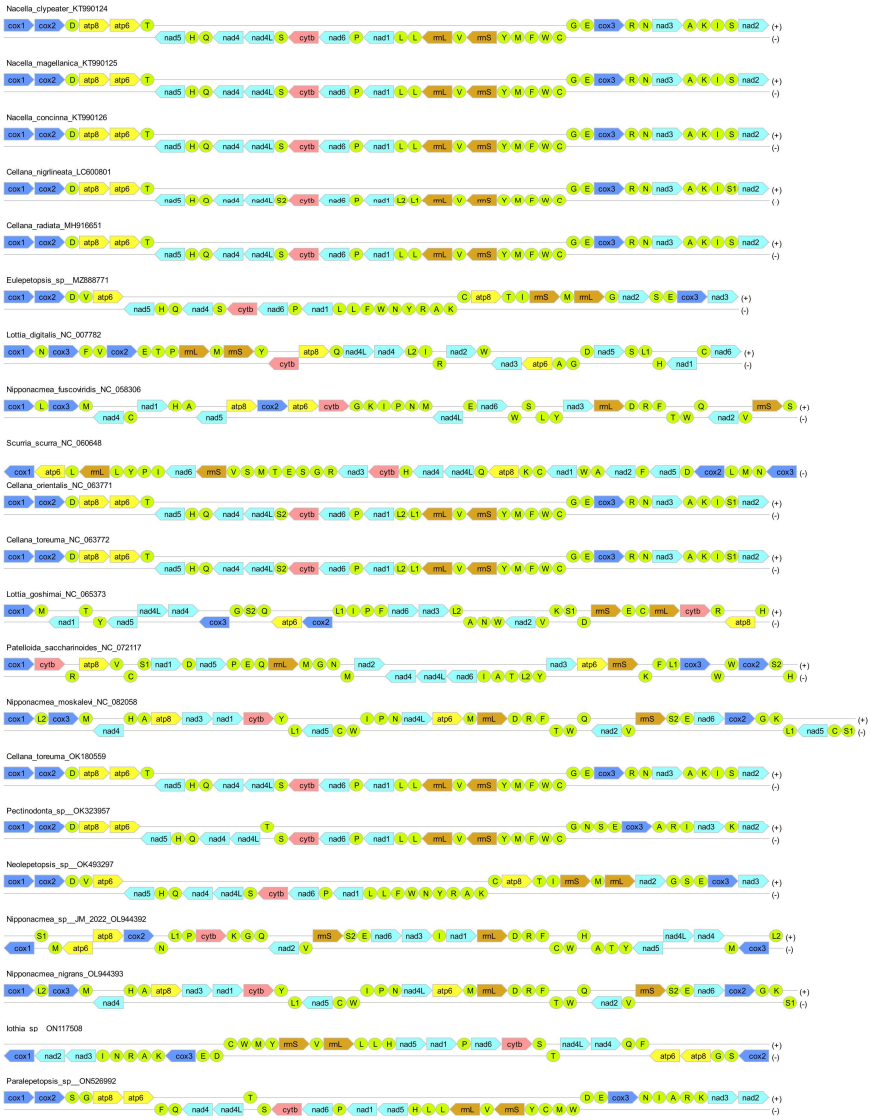

Figure S29. Mitogenomic architectures of all Lottioidea GenBank entries.

Bivalvia: In the molluscan class Bivalvia, within the Protobranchia, which is the sister clade to all other bivalvian lineages [72,76], Solemyida and Nuculida orders exhibited double-stranded mitogenomic architectures, whereas Nuculanida (represented by two mitogenomes belonging to a single species: *Yoldia hyperborea*) exhibited single-stranded architectures (Figure S30). Aside from single-stranded architectures in two *Yoldia hyperborea* mitogenomes, all other mitogenomes (comprising Solemyida, Nuculida and Nuculanida) were double-stranded. As Nuculanida is derived within the Protobranchia [77], we inferred double-stranded architecture as the ancestral state for Protobranchia, and all Bivalvia, and one double-to-single evolutionary transition in *Y. hyperborea* (putatively all Yoldiidae or even Nuculanida) (Figure S30). The shift comprised multiple genes, comprising PCGs and both rRNAs. Notably, the two available conspecific *Y. hyperborea* mitogenomes exhibited a rearrangement of

cox2 and multiple tRNA genes, which may be indicative of common recombination in this species. Due to the sparsity of data, we cannot determine the phylogenetic timing of this event with confidence.

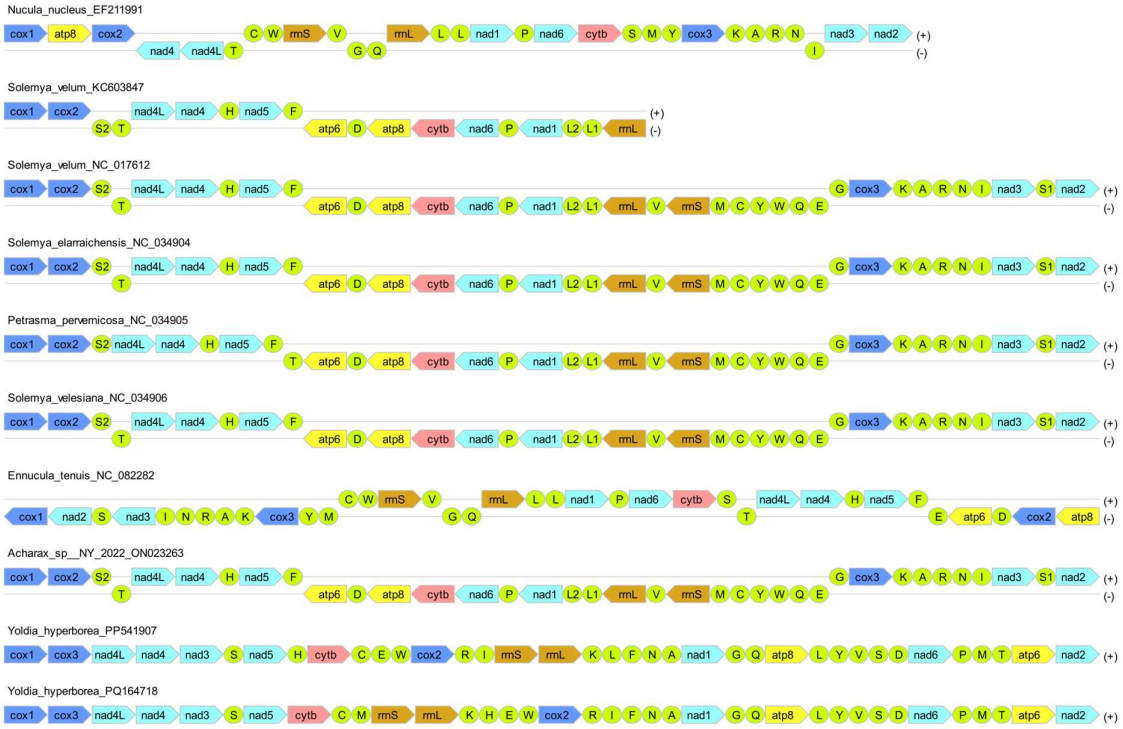

Figure S30. Mitogenomic architectures of all Protobranchia.

As regards the bivalvian class Heteroconchia, the ancestral state is double-stranded, as Palaeoheterodonta (e.g. Unionida; Figure S31) consistently exhibited double-stranded architectures, but we inferred a transition from the ancestral double-stranded architecture (double-to-single event) in the common ancestor of the subterclass Euheterodonta, as a majority of species in both of its superorders, Anomalodesmata (smaller) and Imparidentia (larger) [76], exhibited single-stranded architectures (Figure S32). Two outlier lineages were observed within the Imparidentia. The only available species in the order Galeommatida (*Scintilla* sp.) exhibited a double-stranded architecture (with multiple genes on the minus strand; Figure S33). We should also mention that *Panopea japonica* exhibited a single tRNA gene on the minus strand, but this could easily be an annotation artefact as the mitogenome is incomplete and other *Panopea* species exhibit single-stranded architectures (Figure S33). As mitogenomes are absent for the sister order Gastrochaenida, the event can be mapped anywhere between the ancestor of a single species (*Scintilla* sp.) to the common ancestor of these two orders (Galeommatida+Gastrochaenida). Although these two orders are relatively early-diverging within the Imparidentia, the putatively oldest radiation in this superorder, the order Lucinida

[76], exhibits a single-stranded architecture (Figure S33), so single-stranded is the most parsimonious ancestral state for Imparidentia.

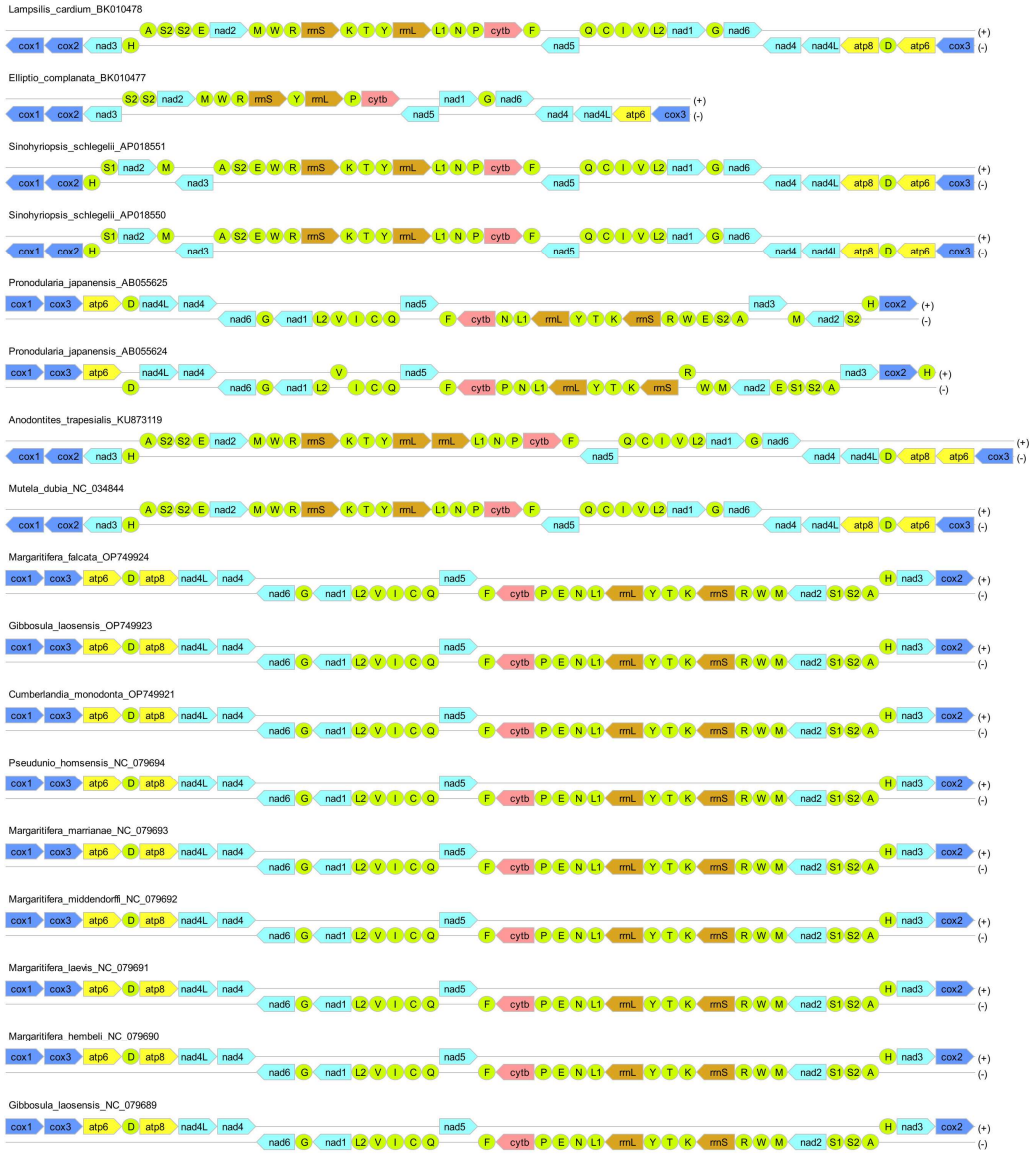

Figure S31. Mitogenomic architectures of a random selection of Unionida (Palaeoheterodonta).

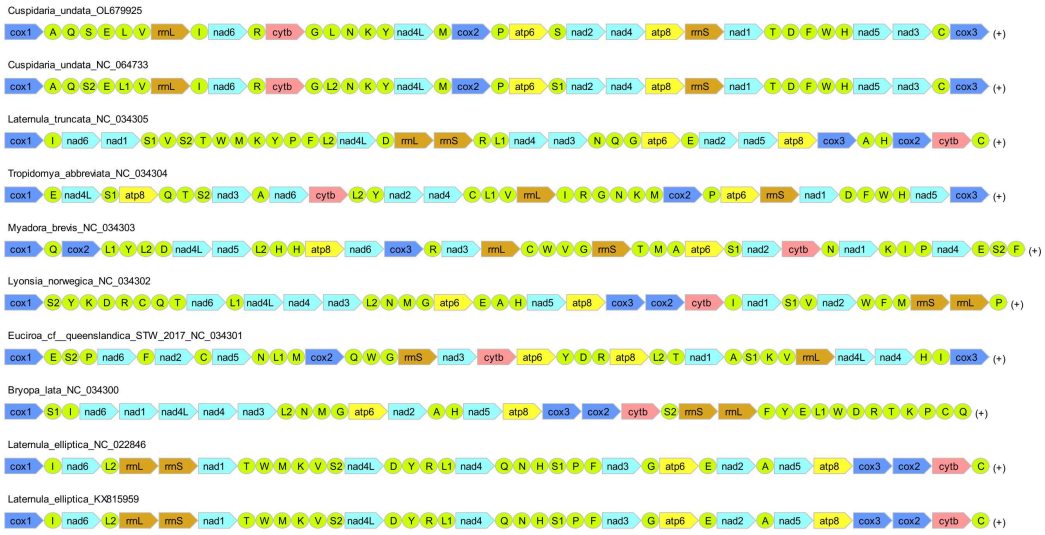

Figure S32. Mitogenomic architectures of all Anomalodesmata.

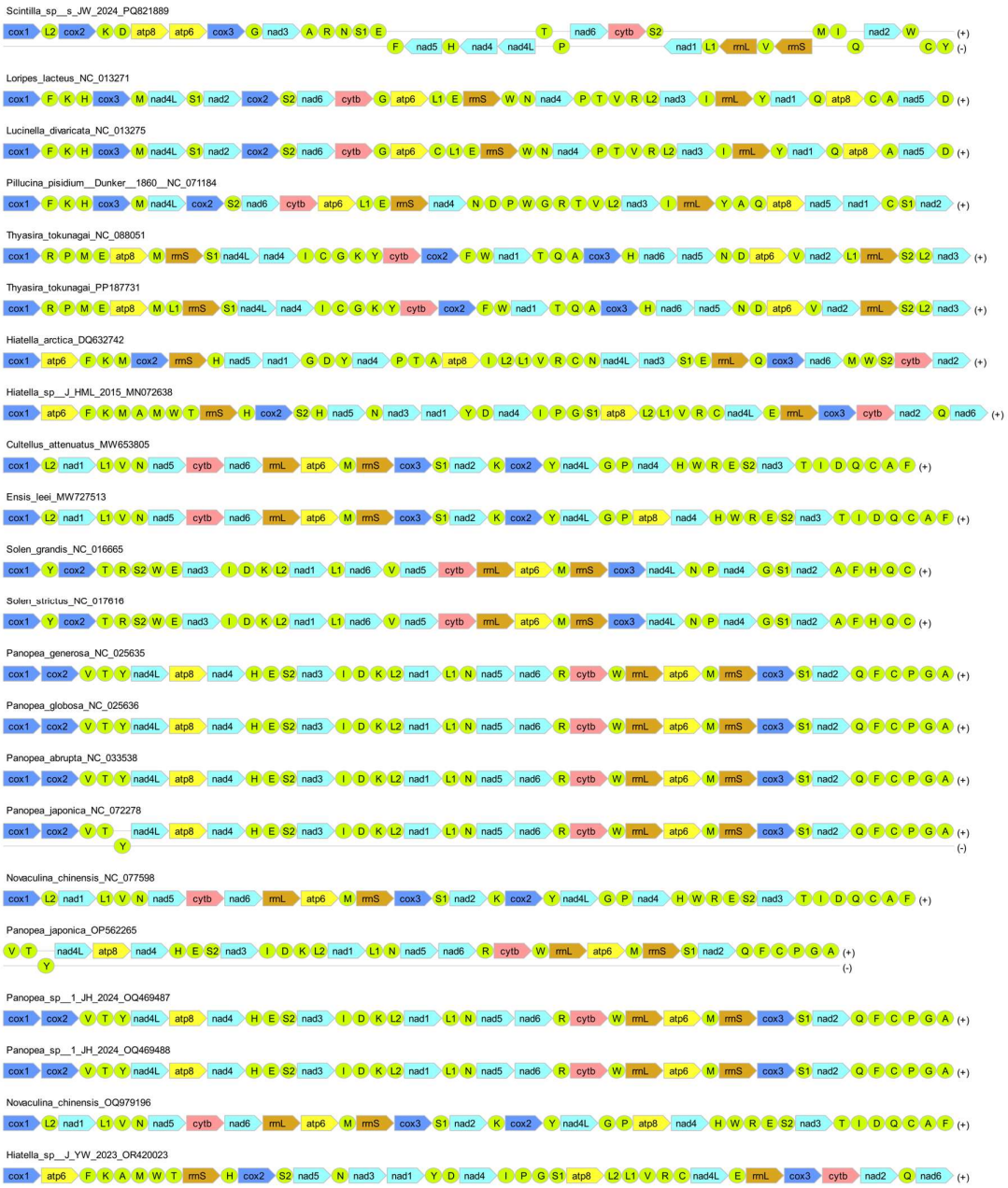

Figure S33. Mitogenomic architectures of "basal" [76] radiations of Imparidentia: Lucinida, Galeommatida, and Adapedonta.

Within the order Myida, all species exhibited a single-stranded architecture, apart from the superfamily Dreissenoidea. All mitogenomes in this lineages were double-stranded, with multiple genes on the minus strand, but the exact phylogenetic location of the shift cannot be determined due to the lineage being represented by only two genera: *Dreissena* and *Mytilopsis* (both family Dreissenidae) (Figure S34).

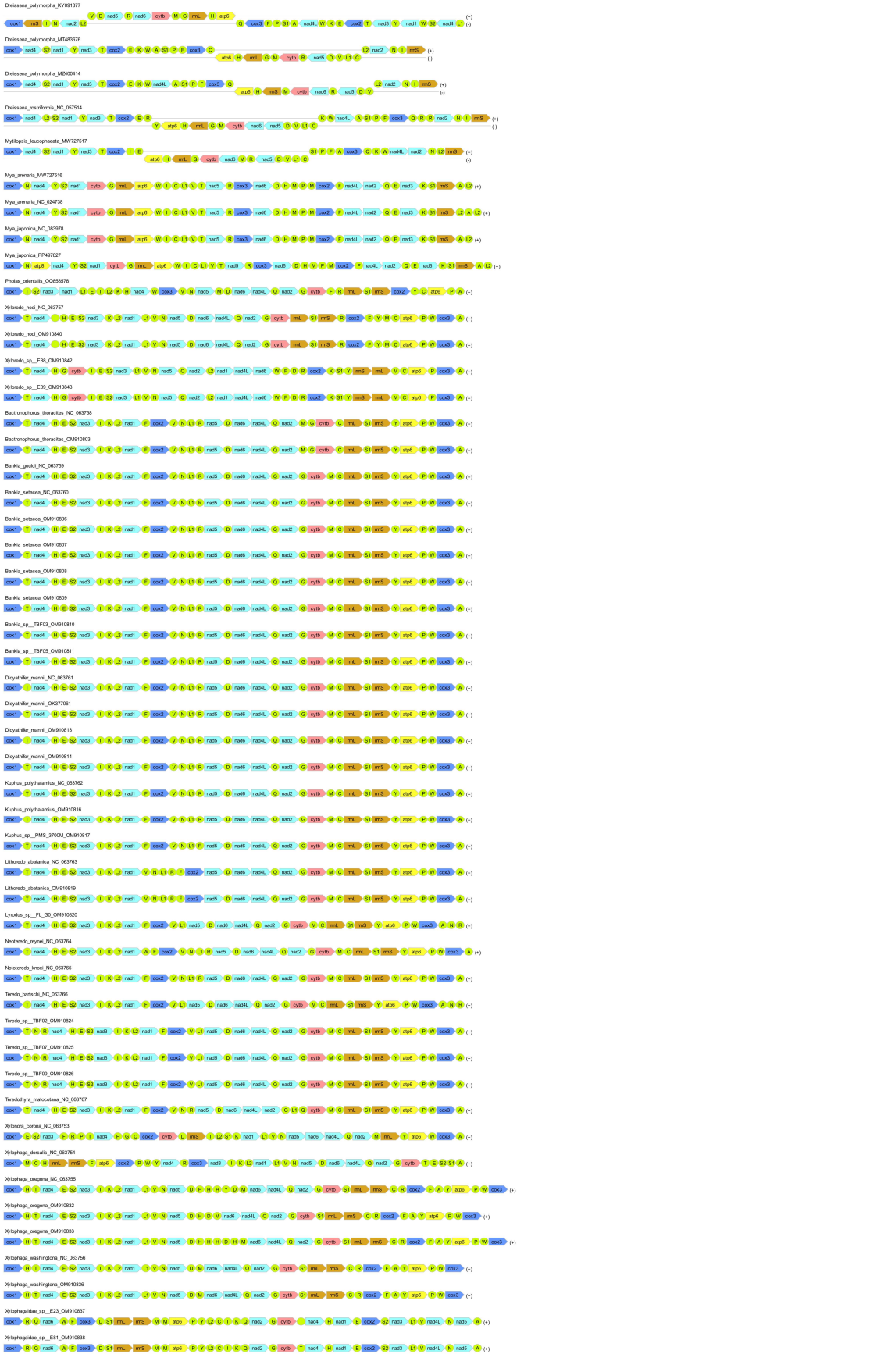
Dreissena_polymorpha_KY091877
Dreissena_polymorpha_MT483676
Dreissena_polymorpha_MZ900414
Dreissena_rostriformis_NC_057514
Mytilopsis_leucophaeata_MW727517
Mya_arenaria_MW727516
Mya_arenaria_NC_024738
Mya_japonica_NC_083978
Mya_japonica_PP497827
Pholas_orientalis_OQ858578
Xyloredo_nooi_NC_063757
Xyloredo_nooi_OM910840
Xyloredo_sp__E88_OM910842
Xyloredo_sp__E89_OM910843
Bactronophorus_thoracites_NC_063758
Bactronophorus_thoracites_OM910803
Bankia_gouldi_NC_063759
Bankia_setacea_NC_063760
Bankia_setacea_OM910806
Bankia_setacea_OM910807
Bankia_setacea_OM910808
Bankia_setacea_OM910809
Bankia_sp__TBF03_OM910810
Bankia_sp__TBF05_OM910811
Dicyathifer_mannii_NC_063761
Dicyathifer_mannii_OK377061
Dicyathifer_mannii_OM910813
Dicyathifer_mannii_OM910814
Kuphus_polythalamius_NC_063762
Kuphus_polythalamius_OM910816
Kuphus_sp__PMS_3700M_OM910817
Lithoredo_abatanica_NC_063763
Lithoredo_abatanica_OM910819
Lyrodus_sp__FL_G0_OM910820
Neoteredo_reynei_NC_063764
Nototeredo_knoxi_NC_063765
Teredo_bartschi_NC_063766
Teredo_sp__TBF02_OM910824
Teredo_sp__TBF07_OM910825
Teredo_sp__TBF09_OM910826
Teredothyra_matoccitana_NC_063767
Xylonora_corona_NC_063753
Xylophaga_dorsalis_NC_063754
Xylophaga_oregona_NC_063755
Xylophaga_oregona_OM910832
Xylophaga_oregona_OM910833
Xylophaga_washingtona_NC_063756
Xylophaga_washingtona_OM910836
Xylophagaidae_sp__E23_OM910837
Xylophagaidae_sp__E81_OM910838

Figure S34. Mitogenomic architectures of the order Myida (Imparidentia).

Finally, we inferred a double-to-single evolutionary transition in the common ancestor of the bivalvian subclass Pteriomorphia, comprising the orders: Pectinida, Limida, Ostreida, Arcida (syn. Arcoida). The vast majority of species exhibited single-stranded architectures (e.g. Figure S35). Within the family Arcidae (Pteriomorphia: Arcida), we observed three *Anadara* species with a few tRNA genes on the minus strand (Figure S36). However, other congenerics and even conspecifics exhibited single-stranded architectures, so these could be assembly or annotation artefacts, or nonfunctional remnants of recent rearrangements events.

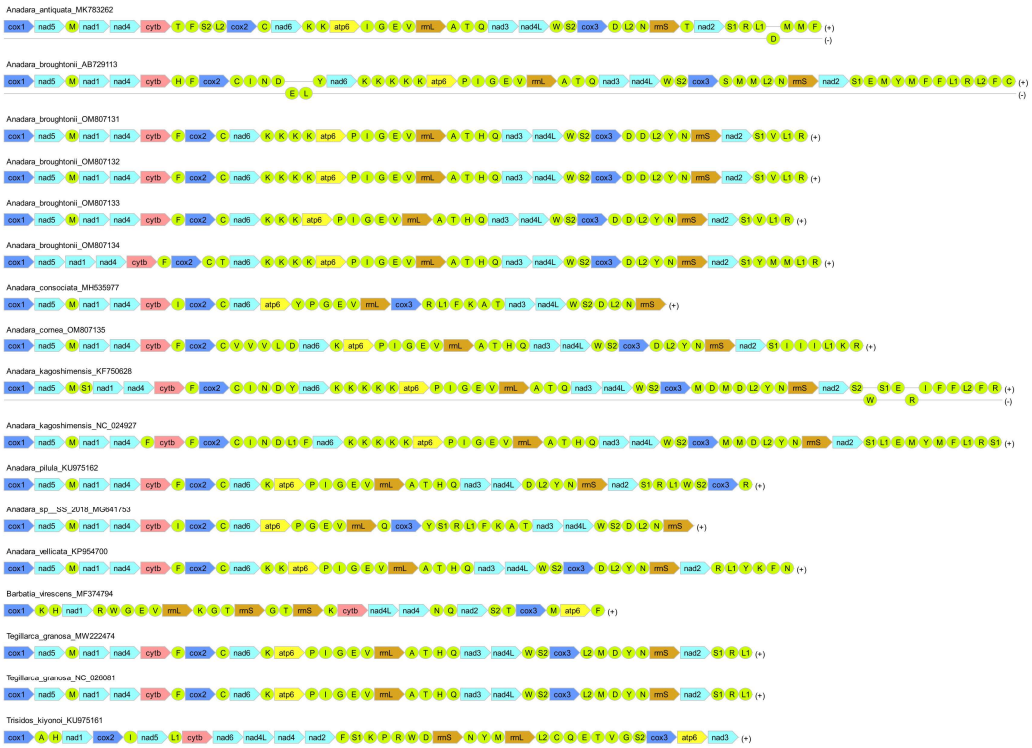

Figure S35. Mitogenomic architectures of the family Arcidae (Pteriomorphia: Arcida).

All Mytiloida species belonged to Mytilidae, which might be divided into two clades: clade 1 and 2 [78]. ***Mytildae Clade 1*:** Subfamilies: Limnoperninae(Litophaginae(Modiolinae+Bathymodiolinae)) [78]. Limnoperninae (*Limnoperna fortunei*) and Litophaginae (*Litophaga kurta*) exhibited the ancestral single-stranded architectures (Figure S36), so the most likely ancestral state for Clade 1 is also single-stranded. A majority of mitogenomes from the Bathymodiolinae (*Bathymodiolus+ Gigantidas* genera) and Modiolinae (*Modiolus*) subfamilies, exhibited *trnT* translocated to the minus strand. Such high level of conservation indicates that gene might be functional and that this may represent a true transition in strandedness, but we cannot confirm this with certainty. The putative transition was mapped to the ancestor of these two subfamilies. Among the nine *Bathymodiolous* species, *Bathymodiolus brooksi* and *Bathymodiolus thermophilus* exhibited apparent single-stranded architectures, with *trnT* encoded on the plus strand. Neither of the studies that reported mitogenomes of these two species did not discuss this discrepancy [78,79], so we suspect that both may be annotation artefacts. Among the seven *Modiolus* species, *M. auriculatus* and *M. modiolus* exhibited apparent single-stranded architectures, with *trnT* encoded on the plus strand. Between the two associated studies [80,81], the one associated with *M. modiolus* mentioned that there was a string of duplicated *trnT* genes [80]. We cannot assess with certainty whether this species underwent another evolutionary shift (back to single-stranded). Remarkably, a series of duplicated tRNA genes, but encoded on the minus strand, was reported in several *Gigantidas* species (Figure S36).

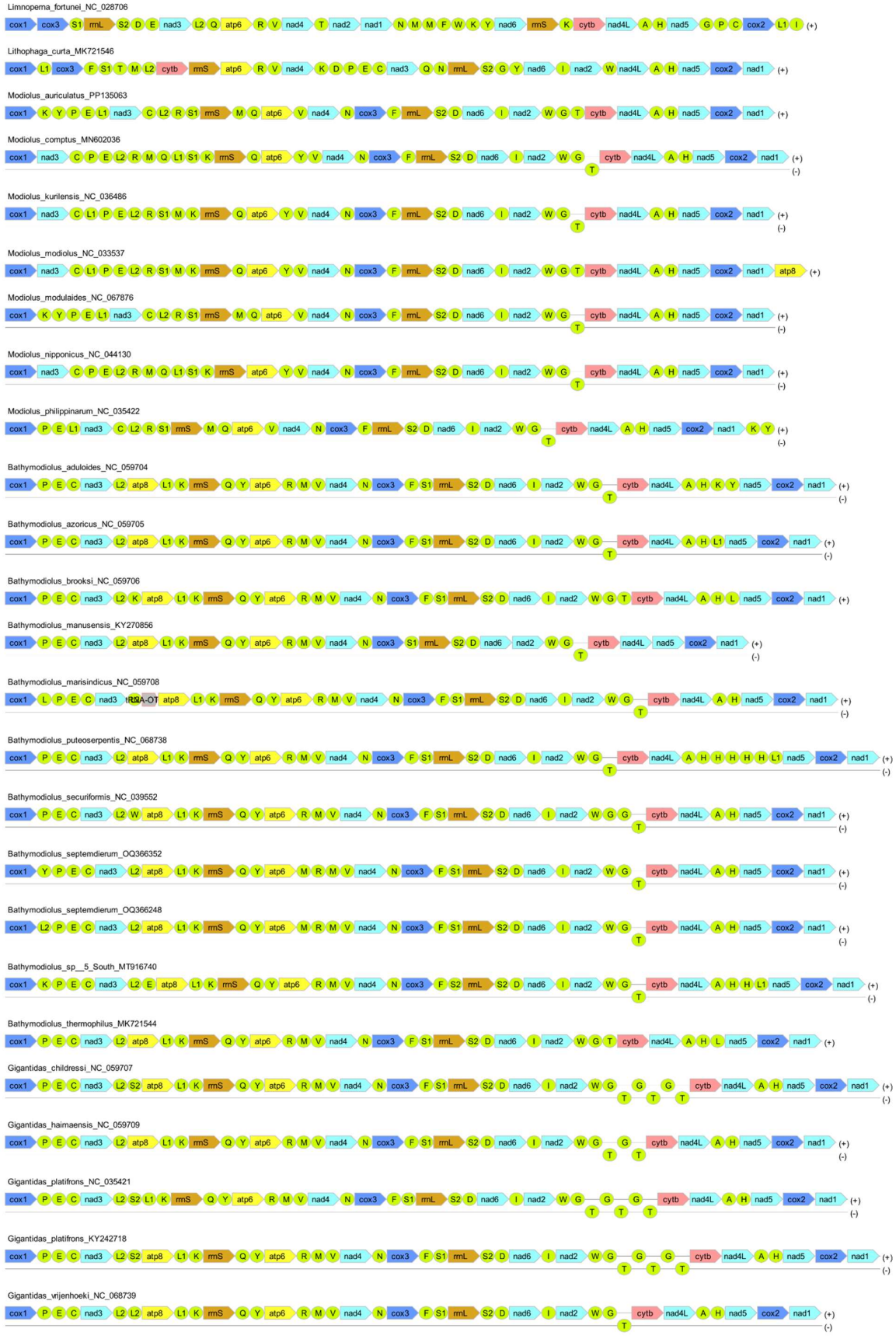
Limnoperna_fortunei_NC_028706
Lithophaga_curta_MK721546
Modiolus_auriculatus_PP135063
Modiolus_comptus_MN602036
Modiolus_kurilensis_NC_036486
Modiolus_modiolus_NC_033537
Modiolus_modulaides_NC_067876
Modiolus_nipponicus_NC_044130
Modiolus_philippinarum_NC_035422
Bathymodiolus_aduloides_NC_059704
Bathymodiolus_azoricus_NC_059705
Bathymodiolus_brooksi_NC_059706
Bathymodiolus_manusensis_KY270856
Bathymodiolus_marisindicus_NC_059708
Bathymodiolus_puteoserpentis_NC_068738
Bathymodiolus_securiformis_NC_039552
Bathymodiolus_septemdierum_OQ366352
Bathymodiolus_septemdierum_OQ366248
Bathymodiolus_sp__5_South_MT916740
Bathymodiolus_thermophilus_MK721544
Gigantidas_childressi_NC_059707
Gigantidas_haimaensis_NC_059709
Gigantidas_platifrons_NC_035421
Gigantidas_platifrons_KY242718
Gigantidas_vrijenhoeki_NC_068739

Figure S36. Mytilidae Clade 1**:** Limnoperninae, Litophaginae, Modiolinae and Bathymodiolinae.

Mytilidae Clade 2: Subfamilies and genera in this clade comprise: Brachidontinae (*Brachidontes+Mytilisepta+Perna+Geukensia*), Mytilinae (*Mytilus+Crenomytilus+Perna*); Crenellinae (*Gregariella+ Mytella*), Septiferinae (*Perumytilus+Septifer*) [78,82]. Among these, most mitogenomes were single-stranded (e.g. *Brachidontes*, *Geukensia*, *Gregariella*, *Crenomytilus*, *Perumytilus, Mytillisepta*…), so the ancestral state for Clade 2 of Mytilidae is likely to be single-stranded, as most species exhibited that architecture, and this does not require any changes in the ancestral strand state of Mytilidae. In Crenellinae (Arcuatulinae in NCBI), two out of five *Arcuatula senhousia* mitogenomes exhibited a double-stranded architecture, but only with *trnS2* on the minus strand (Figure S37). As this was not mentioned in a paper that reported both M and F types [83], this may be an annotation artefact. Similar, both *Xenostrobus securis* (Arcuatulinae in NCBI, Xenostrobinae in WORMS) mitogenomes exhibited *trnT* on the minus strand (Figure S38).

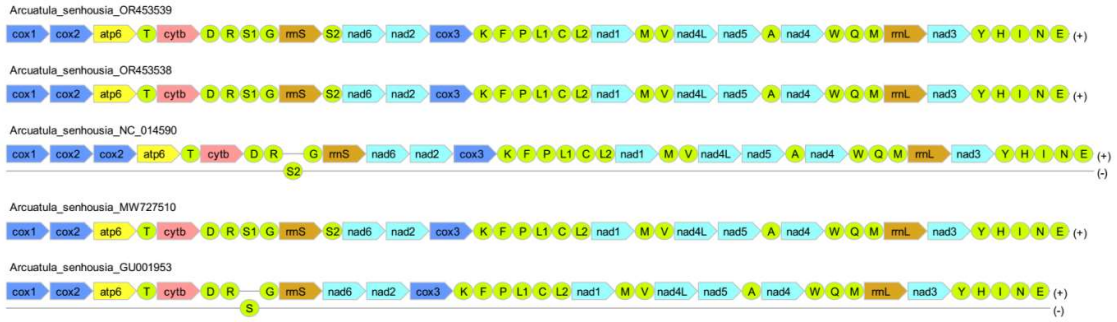

Figure S37. Mytilidae Clade 2**:** *Arcuatula* (Crenellinae in WORMS, Arcuatulinae in NCBI).

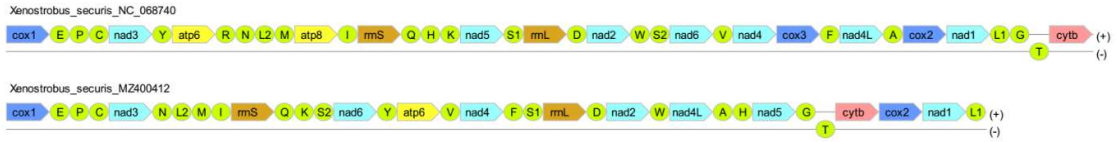

Figure S38. Mytilidae Clade 2**:** *Xenostrobus* (Crenellinae in WORMS, Arcuatulinae in NCBI).

Text S5. GORR values distribution and correlations with branch length, mitogenome size, and strand distribution of genes

Kolmogorov-Smirnov test rejected the hypothesis that GORR distribution across the Bilateria fits an exponential distribution. The correlation between GORR and branch length was unaffected by recoding GORR = 0 values as GORR = 0.0000001: (a) for "0" values, results were r = 0.6892, p = 0.0, and R^2 = 0.4750; (b) for "0.0000001" values, results were: r = 0.6892, p = 0.0, and R^2 = 0.4750. When Chordata were removed from the dataset completely, results were: r = 0.5739, p = 0.0, and R^2 = 0.3293.

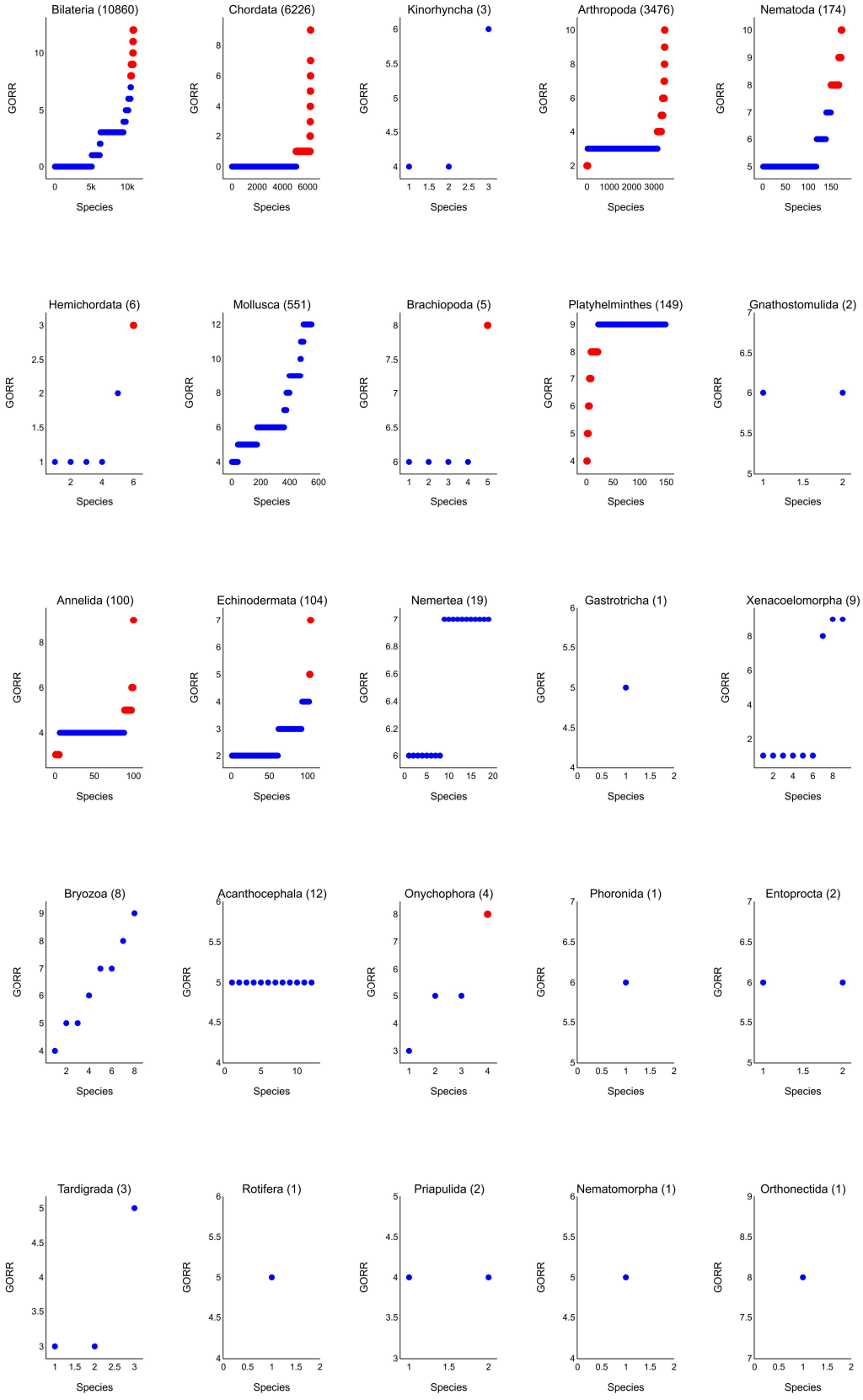
Bilateria (10860)
Chordata (6226)
Kinorhyncha (3)
Arthropoda (3476)
Nematoda (174)
Hemichordata (6)
Mollusca (551)
Brachiopoda (5)
Platyhelminthes (149)
Gnathostomulida (2)
Annelida (100)
Echinodermata (104)
Nemertea (19)
Gastrotricha (1)
Xenacoelomorpha (9)
Bryozoa (8)
Acanthocephala (12)
Onychophora (4)
Phoronida (1)
Entoprocta (2)
Tardigrada (3)
Rotifera (1)
Priapulida (2)
Nematomorpha (1)
Orthonectida (1)
GORR
Species

Figure S39. The distribution of gene order rearrangement rates (GORR) in comparison to the ancestral bilaterian architecture across Bilateria for each phylum. Statistically identified outliers are highlighted in red.

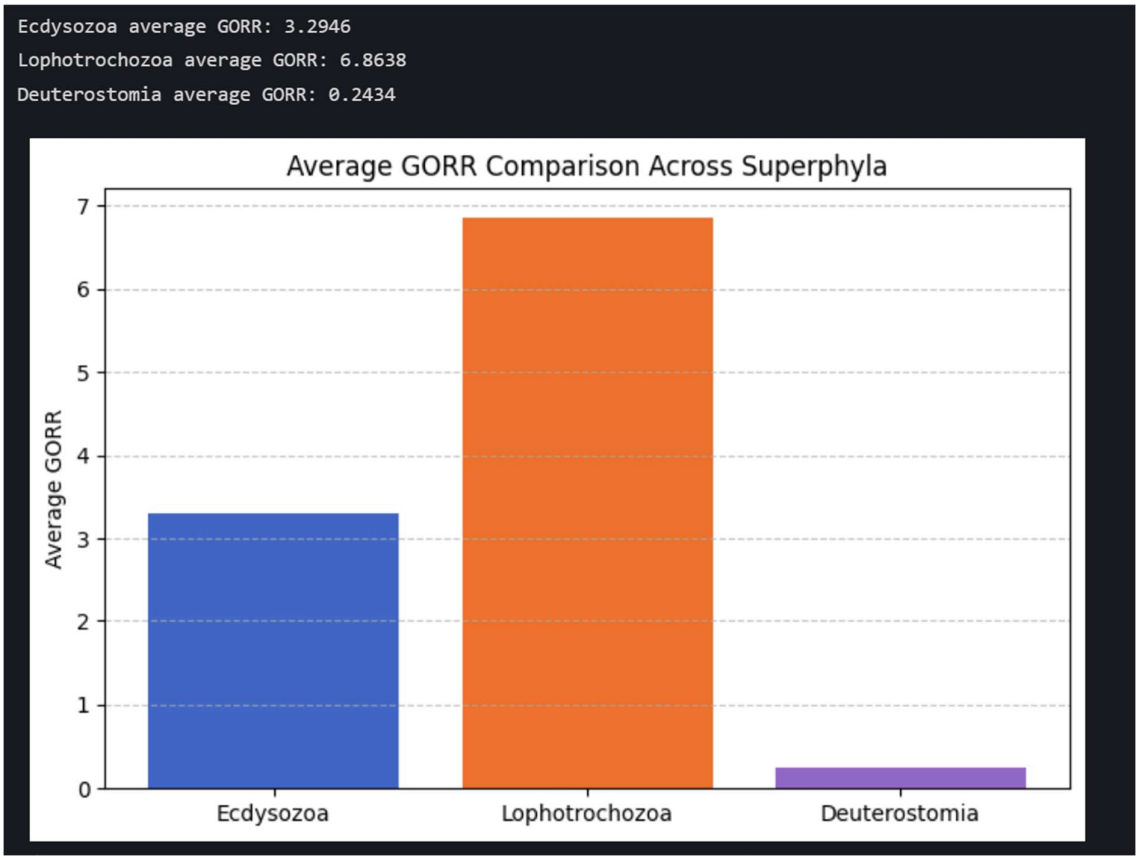

Figure S40. Average gene order rearrangement rate (GORR) values across the three bilaterian superphyla for each phylum.

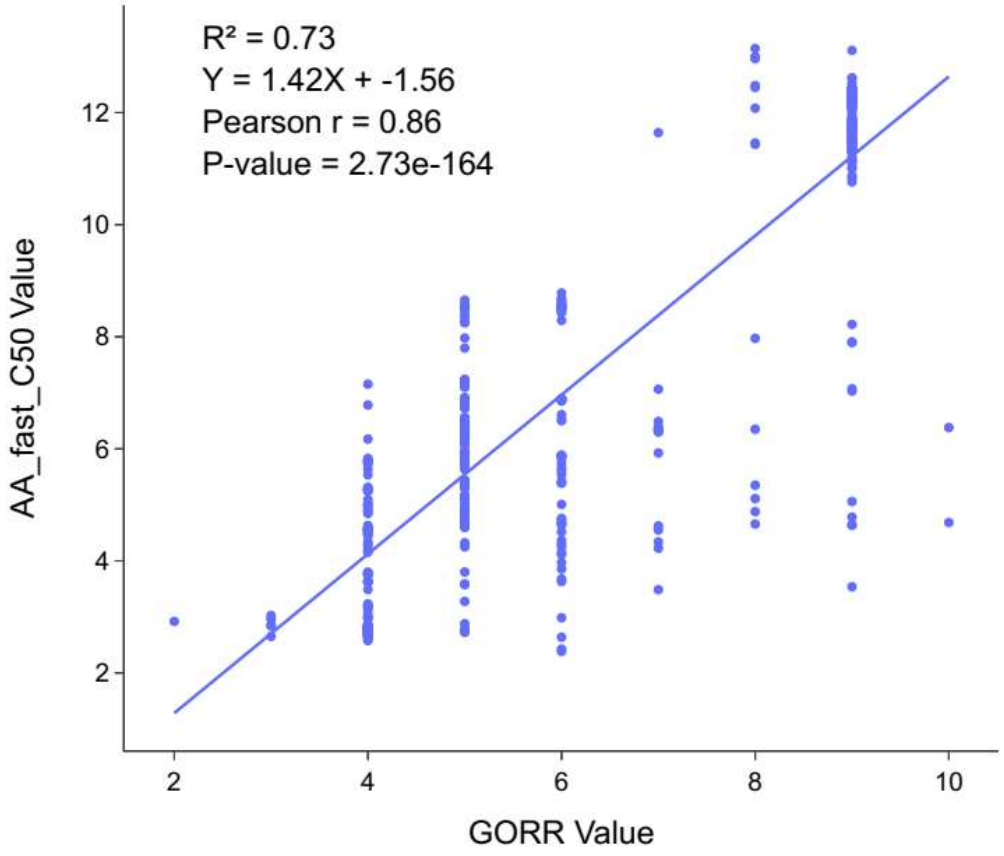

Figure S41. The correlation between the gene order rearrangement rate (GORR) and branch length (AA_fast_C50 Value) inferred using only single-stranded mitogenomes (all genes encoded on a single strand). Correlation is presented as Pearson r, and R^2 is regression. GORR = 0 values were recoded as 0.0000001.

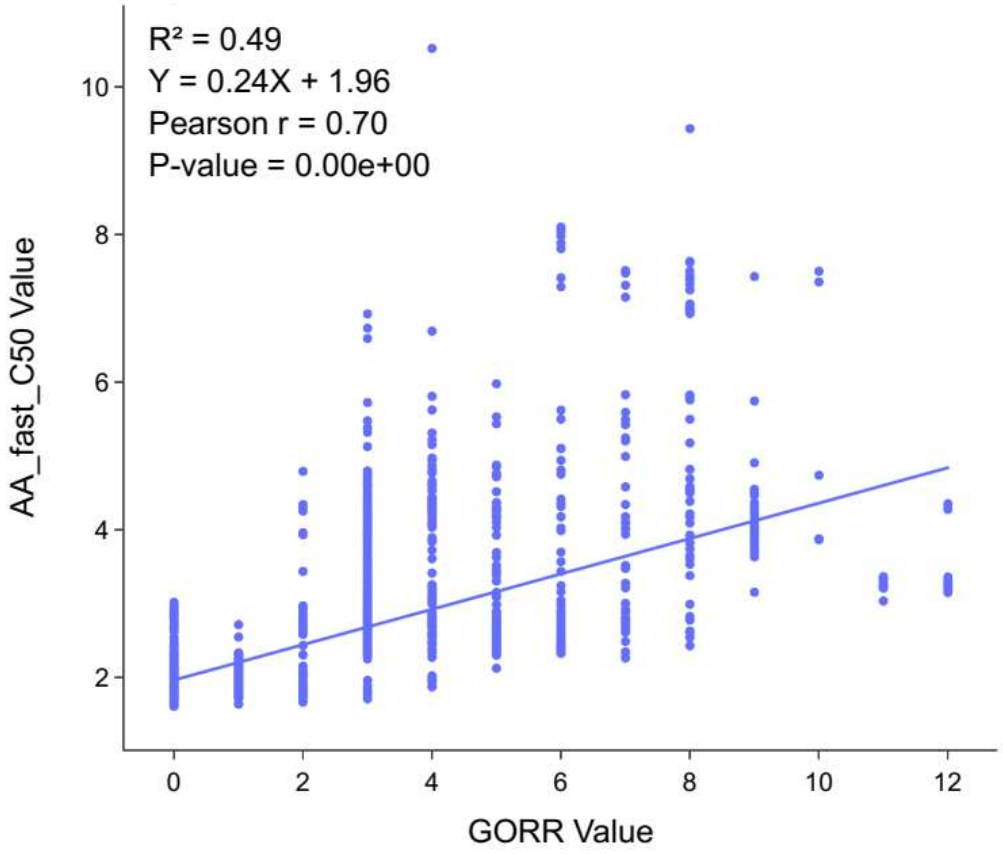

Figure S42. The correlation between the gene order rearrangement rate (GORR) and branch length (AA_fast_C50 Value) inferred using only double-stranded mitogenomes (genes encoded on both strands). Correlation is presented as Pearson r, and R^2 is regression. GORR = 0 values were recoded as 0.0000001.

```
Group GORR >= 7 brl: Count = 421, Mean = 6.77553919239905, Std = 3.7934772936748895
Group GORR < 7 brl: Count = 10439, Mean = 2.409786569594789, Std = 0.8990851795230749
brl comparison between two groups, T-statistic: 76.04687650410519, P-value: 0.0
Correlation (GORR and AA_fast_C50) for GORR >= 7: -0.18414413546920747
Correlation (GORR and AA_fast_C50) for GORR < 7: 0.6897612404439364
```

Figure S43. Details of correlation analyses between GORR and branch length in highly rearranged (GORR≥7) and architecturally conserved (GORR<7) mitogenomes.

```
Statistics for Strand_Trait = double-stranded:
Group Strand_Trait = double-stranded, GORR >= 7: Count = 251, Mean = 4.066641434262948, Std = 1.2876010837663716
Group Strand_Trait = double-stranded, GORR < 7: Count = 10044, Mean = 2.2963877937076864, Std = 0.6192251768379109

Statistics for Strand_Trait = single-stranded:
Group Strand_Trait = single-stranded, GORR >= 7: Count = 170, Mean = 10.77514705882353, Std = 2.514080625685445
Group Strand_Trait = single-stranded, GORR < 7: Count = 395, Mean = 5.293273417721519, Std = 1.7256867260085318

AA_fast_C50 comparison for Strand_Trait = double-stranded, T-statistic: 43.03337488062722, P-value: 0.0
AA_fast_C50 comparison for Strand_Trait = single-stranded, T-statistic: 29.95101284456735, P-value: 1.3467314101702297e-118

Correlation (GORR and AA_fast_C50) for Strand_Trait = double-stranded, GORR >= 7: -0.345015273826854
Correlation (GORR and AA_fast_C50) for Strand_Trait = double-stranded, GORR < 7: 0.6931874402643464
Correlation (GORR and AA_fast_C50) for Strand_Trait = single-stranded, GORR >= 7: 0.5542617737180465
Correlation (GORR and AA_fast_C50) for Strand_Trait = single-stranded, GORR < 7: 0.5951545921388597
```

Figure S44. Details of correlation analyses between GORR and branch length with the full dataset divided into four subdatasets along the lines of strand distribution of genes (single-stranded vs. double-stranded) and rearrangement rate (GORR>7 vs. GORR≤7).

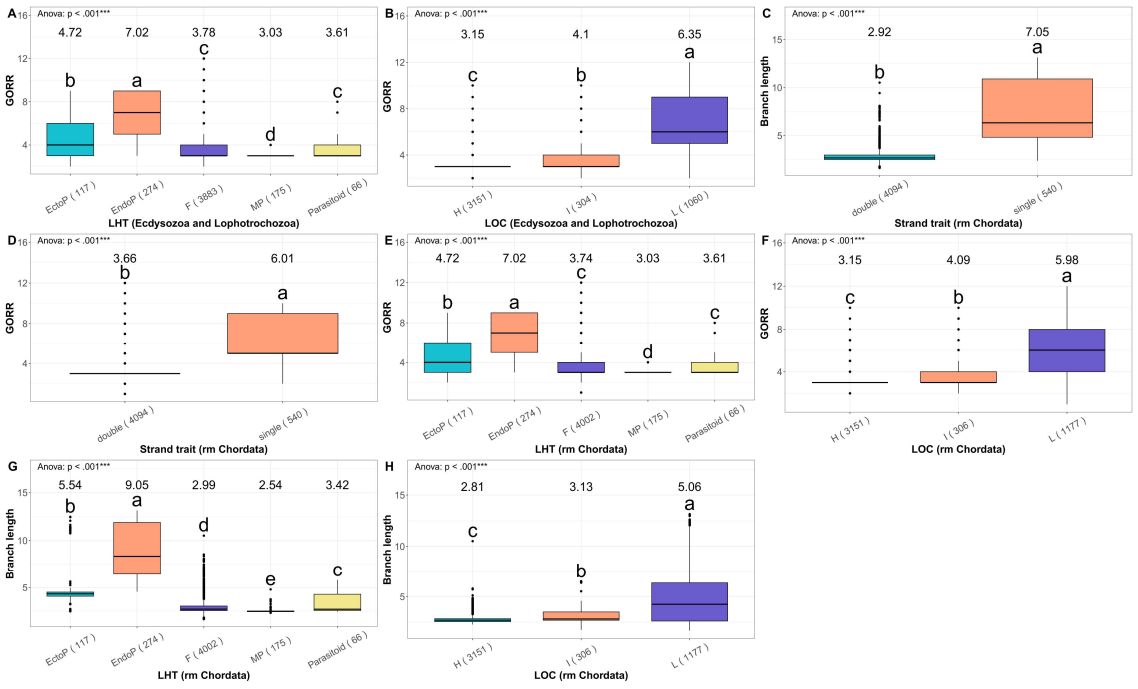

Figure S45. Additional pairwise Tukey HSD tests. In each panel, the GORR/branch length distribution boxplot is shown on the y-axis, while datasets compared are shown on the x-axis. The titles below the panels are presented in the following format: categorisation (dataset). In the life-history (LHT) categorisation, F is free-living, EndoP is endoparasitic, EctoP is ectoparasitic, and MP is micropredatory. In the locomotory capacity (LOC) categorisation, H is high, I is intermediate, and L is low. The number of species included is shown next to the category name. “rm Chordata” indicates that Chordata were removed from the dataset. “Strand trait” panels (C and D) supplement Figure 4 in

the main manuscript, and test the impact of strand distribution of genes on GORR and branch length, with “double” being double-stranded mitogenomes, and “single” single-stranded ones. Boxplots show the minimum, first quartile, median, third quartile, and maximum, plus outliers. Average branch length values are shown above the boxplots. GORR is gene order rearrangement rate. ANOVA results are shown in the upper left corner. Different letters above the boxplots indicate statistically significant differences ($p < 0.05$; Tukey HSD). Details of statistical analyses are provided in Supplementary file 2: Worksheet S3.

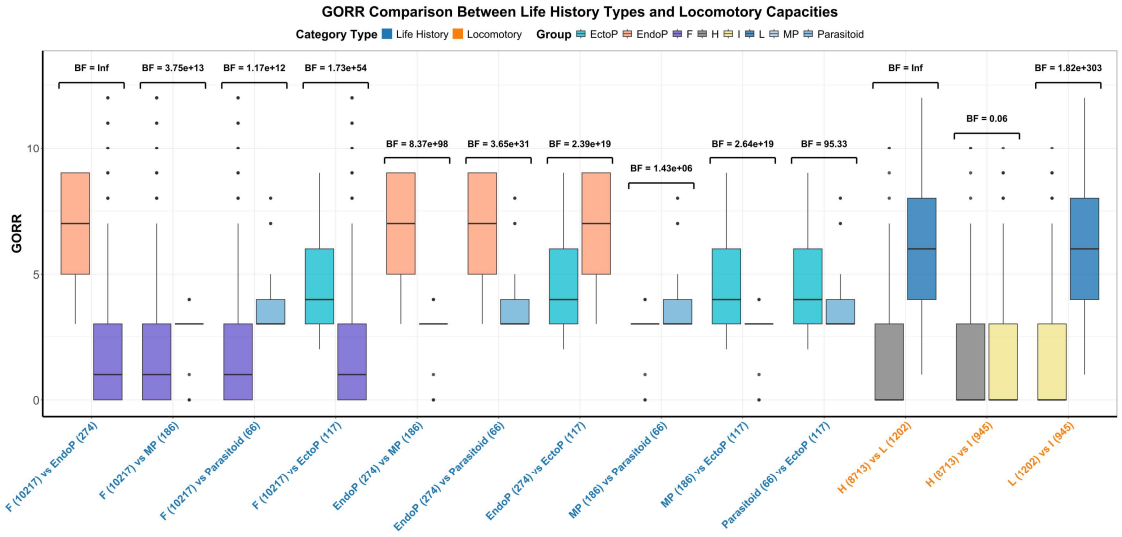

Figure S46. Bayes Factor values for pairwise group comparisons of GORR values among different life history and locomotory capacity categories inferred using a larger *Rscale* prior of 1.0. In the life history categorisation, F is free-living, EndoP is endoparasites, EctoP is ectoparasites, and MP is micropredators. In the locomotory capacity categorisation, H is high, I is intermediate, and L is low.

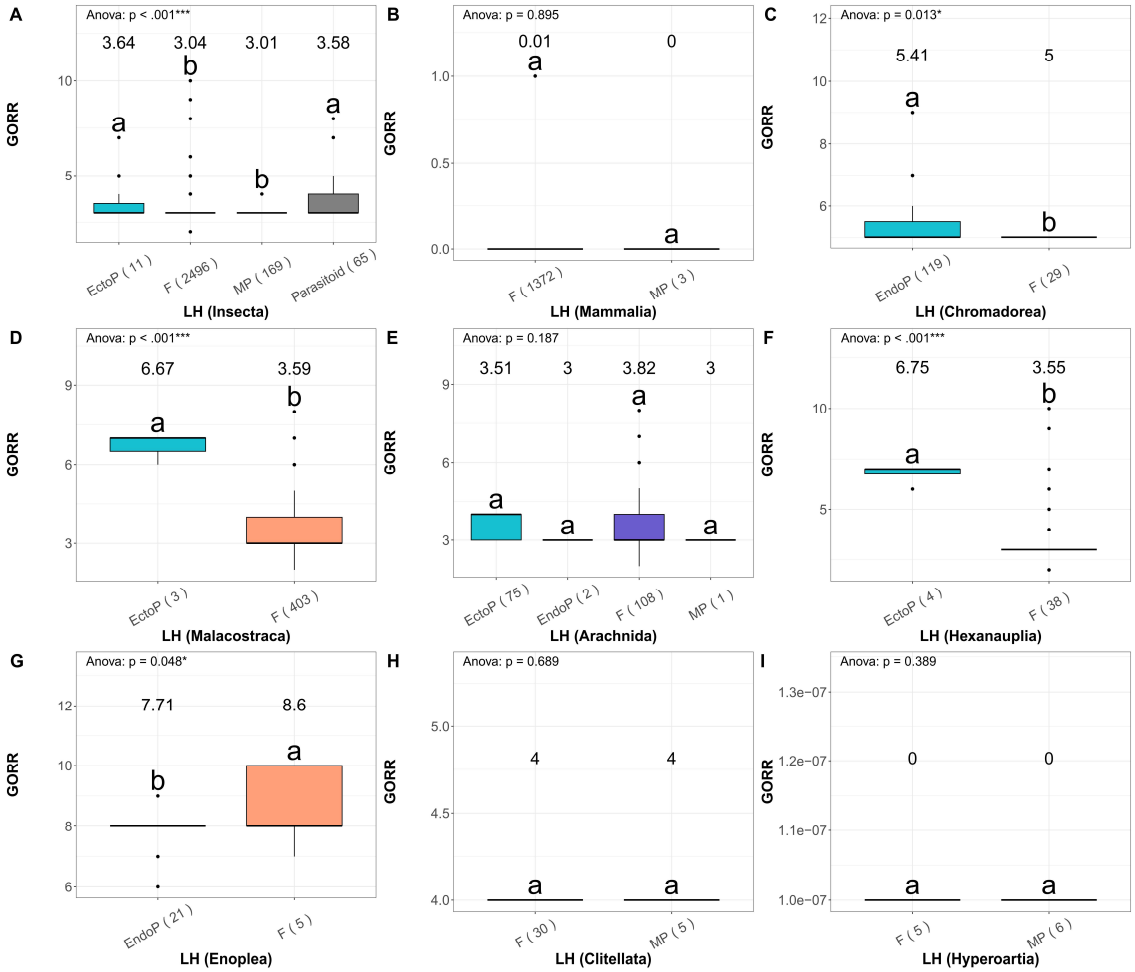

Figure S47. Pairwise comparisons (Tukey HSD tests) of GORR values between different life history categories across individual classes. See Figure S45 for other details.

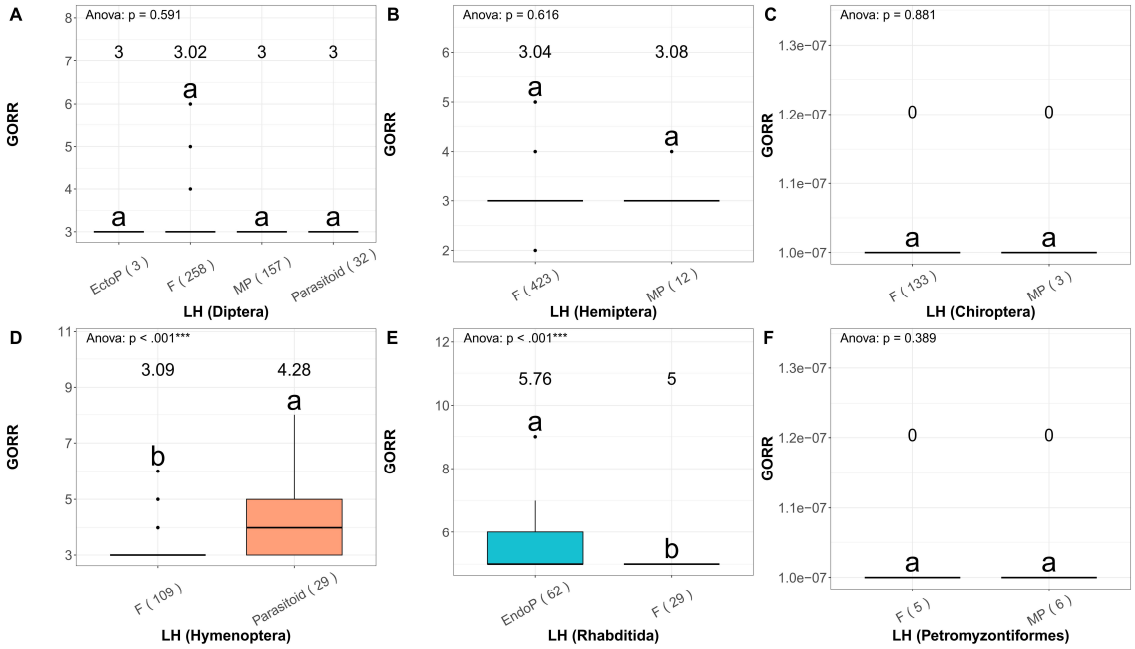

Figure S48. Pairwise comparisons (Tukey HSD tests) of GORR values between different life history categories (LH) across individual orders. See Figure S45 for other details.

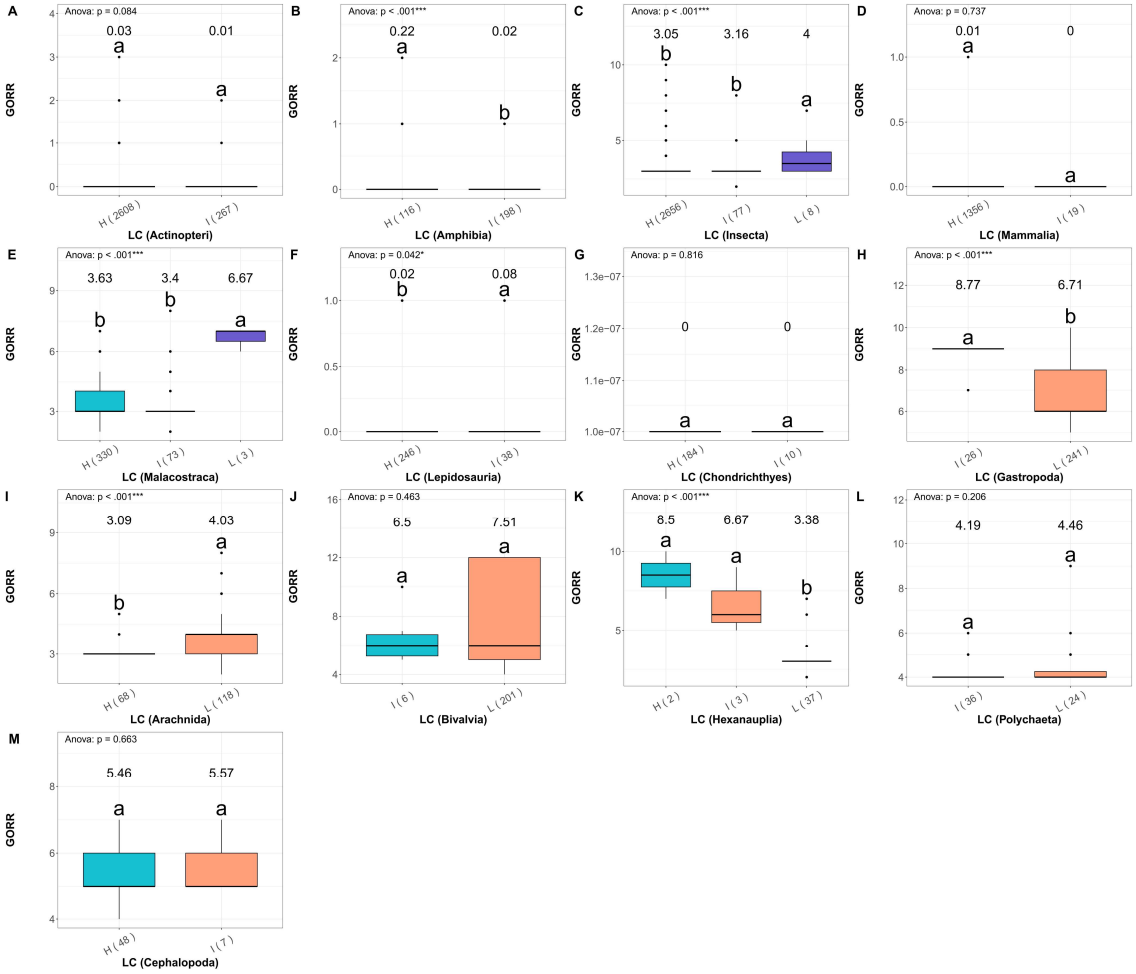

Figure S49. Pairwise comparisons (Tukey HSD tests) of GORR values between different locomotory capacity categories (LH) across individual classes. See Figure S45 for other details.

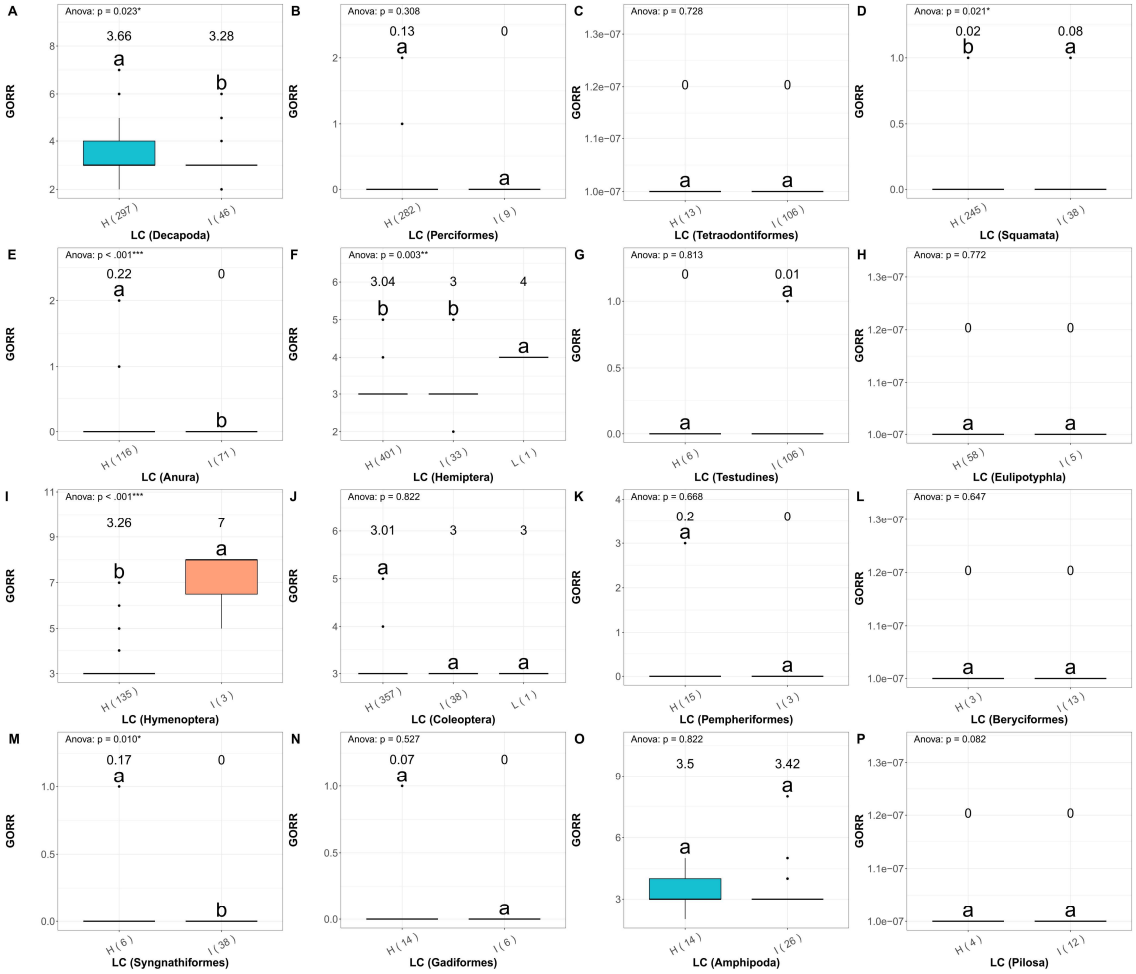

Figure S50. Pairwise comparisons (Tukey HSD tests) of GORR values between different locomotory capacity categories (LH) across individual orders. See Figure S45 for other details.

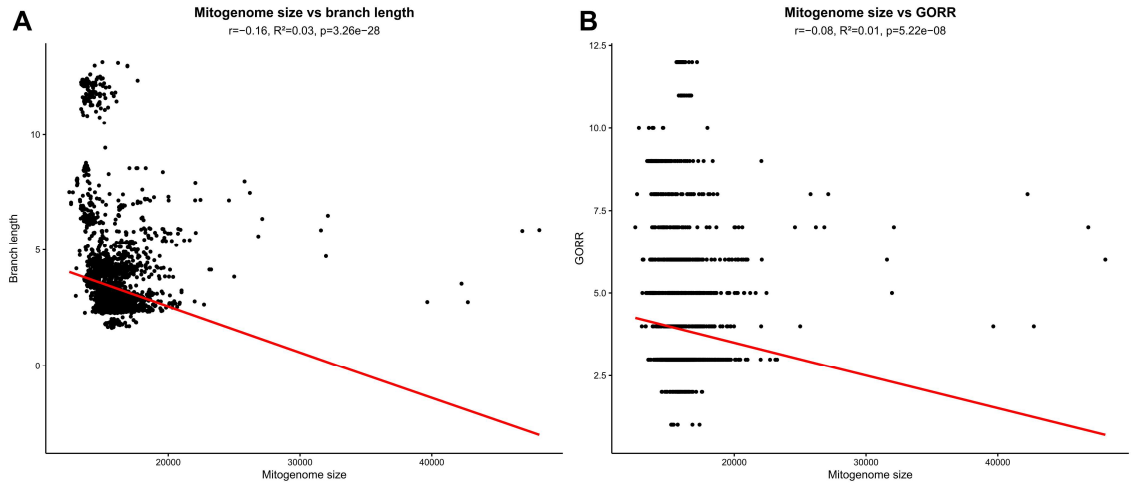

Figure S51. Correlations between the mitogenome size and branch length (panel A) and gene order rearrangement rate (GORR) (panels B), with Chordata removed from the dataset. Correlation is presented as Pearson r, and R^2 is regression. GORR = 0 values were recoded as 0.0000001.

Text S6. Ancestral architectural types in Lophotrochozoa

Podsiadlowski et al. [42] based the argument that the ancestral state for Lophotrochozoa was single-stranded on the observation that "Brachiopoda, Annelida, Platyhelminthes and Acanthocephala all have single-strand architectural types". In partial contradiction, our inference produced double-stranded architecture as the most likely ancestral state for all lophotrochozoan phyla aside from Brachiopoda and Acanthocephala, so this discrepancy needs to be discussed in more detail.

As regards the two phyla where our ancestral state inference is in disagreement with the reconstruction of Podsiadlowski et al. [42], we inferred double-stranded as the most parsimonious ancestral architecture for Annelida and Platyhelminthes (flatworms) on the basis of "basal" lineages of both phyla exhibiting double-stranded architectures. Despite the vast majority of Platyhelminthes exhibiting a single-stranded architecture, we inferred a double-stranded ancestral architecture for this phylum, because both available mitogenomes in the "basal" radiation (i.e. sister clade to all other Platyhelminthes), Catenulida [65,66], exhibited a double-stranded architecture [67] (Figure S13). In this scenario, only one double-to-single transition is required in the common ancestor of the remaining Platyhelminthes ("turbellaria+Neodermata", all single-stranded), whereas in the alternative scenario, a double-to-single transitions would be required in the ur-Lophotrochozoa, followed by the evolutionarily very rare single-to-double transition in the Catenulida. For Annelida, Oweniidae and Magelonidae exhibit double-stranded architectures, and this was recognised as the most likely ancestral state for the entire phylum [84]. The same rationale was applied to infer double-stranded as the ancestral state in the remaining two phyla exhibiting complex evolutionary scenarios in this aspect: Mollusca and Bryozoa. In addition, we should note that we extended the transition to single-strandedness from Acanthocephala to Syndermata (comprises Rotifera as well). Among the Rotifera, now recognised as paraphyletic [85,86], some species exhibited both single-stranded and double-stranded mitogenomes (*Asplanchna brigtwelli*, *Brachionus calyciflorus*, and *B. plicatilis*;

Figure S12). As rotifers also predominantly exhibit fragmented mitogenomes [87], we cannot ascertain with confidence whether these are assembly or annotation artefacts, or state reversals (single-to-double architectural transitions). Syndermata is a derived phylum within the superclade Gnathifera [62], wherein both other phyla, Chaetognatha and Gnathostomulida, have double-stranded ancestral architectures, which makes double-stranded the most parsimonious ancestral state for Gnathifera. Similarly, the most likely sister-clades to other discussed phyla, Gastrotricha (Platyhelminthes), Orthonectida (Annelida), Nemertea (Mollusca), and Phoronida (Bryozoa), all have double-stranded architectures [42,61,88,89]. Combined, these findings further support double-stranded as the ancestral state for Lophotrochozoa.

Text S7. Parasitoids, ectoparasites with high locomotory capacity, and GC skews

Further support for our proposed model of mitogenomic evolution was found in parasitoids exhibiting intermediate GORR values. This supports our previous hypothesis and observation that due to the selection for high locomotory capacity in adults, parasitoids should have lower evolutionary rates than most other parasites [24]. In addition, we also found that ectoparasites with high locomotory capacity had lower GORR values than those with low locomotory capacity, which further mirrors our previous hypotheses and sequence evolution analyses [24]. Previously we proposed that GC skew is a more reliable measure of purifying selection pressure in crustacean mitogenomes than dN/dS ratio, largely due to the parameter-rich and often noisy calculation of the latter [90]. In support of this hypothesis, herein we found an intermediate, highly significant, positive correlation of GORR with GC skew and AT content (Figure S52). We should note that the actual correlation is likely to be much higher, because did not identify putative strand switches of the origin of replication in our dataset, which beyond any doubt produced a huge amount of noise in the analysis and almost certainly reduced the inferred magnitude of the correlation. For further details of these issues please see [90,91]. We should also mention here that Struck et al. [45] also found that GC skew had a very high explanatory power on architectural rearrangement rates in their analyses of annelid mitogenomes. Therefore, this is another piece of evidence supporting the major role of purifying selection in mitogenomic architectural evolution.

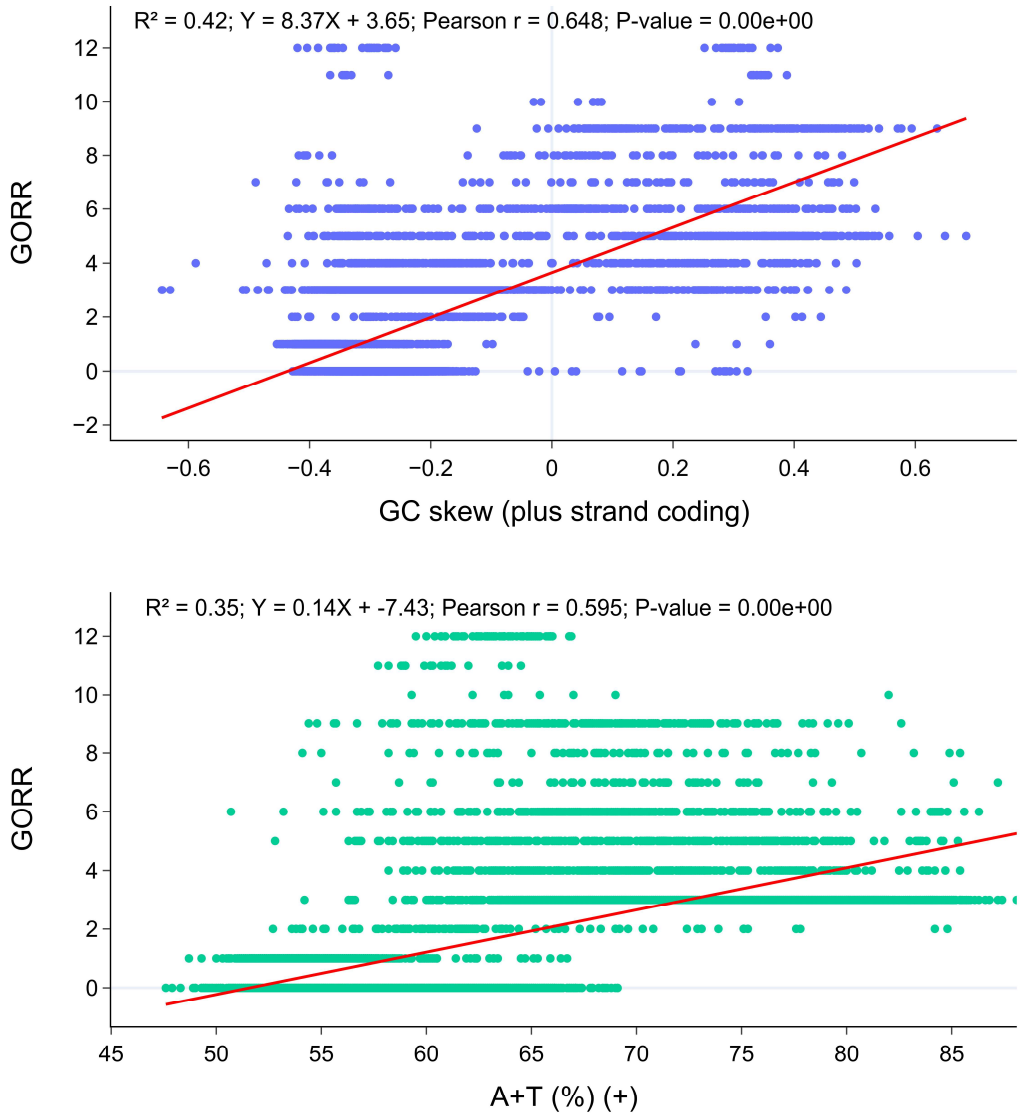

Figure S52. Correlations between the GORR and GC skew (upper panel; calculated using only the coding section of the mitogenomic plus strand) and A+T content (lower panel; calculated using the entire mitogenomic plus strand). Correlation is presented as Pearson r, and R^2 is regression. GORR = 0 values were recoded as 0.0000001.

Text S8. Rejects, outliers and limitations

The correlation between GORR and branch length disappeared in highly rearranged mitogenomes with double-stranded architectures (it was found in all other tested combinations). This appears to contradict the results of Bernt et al. [47], but results are not directly comparable as they studied a much smaller dataset (650 vs. 10,860 mitogenomes), and they only statistically tested the correlation on the overall dataset, without testing subdatasets statistically: "Complete shuffling of the mitochondrial genome is clearly correlated with long branches (equals high substitution rate), while a moderate gene rearrangement (2–6 breakpoints) has virtually no effect." [47]. Notably, in the overall dataset, they obtained an identical value to the one found in our analyses (r = 0.69). We hypothesise that the disappearing correlation between GORR and branch length in highly rearranged mitogenomes with double-stranded architectures this may indicate that purifying selection pressures acting on rearrangements, but not on sequence mutations, become highly weakened (to the point of disappearing) in lineages exhibiting highly rearranged mitogenomes. This is not a stretch, as nonsynonymous sequence mutations may severely negatively affect the functioning of the OXPHOS cycle even in lineages evolving under relaxed selection pressures, whereas gene order rearrangements per se would have much lower impacts on fitness in lineages with already destabilized architectures. Of course, architectural rearrangements causing fragmentation of key genes would still be lethal in most cases, as reflected in the gene (PCGs+rRNAs) content remaining relatively stable throughout the evolution of bilaterian animals (although there is evidence of losses of individual genes in isolated lineages) [43,92]. Indeed, in our analyses of parasitic mitogenomes, we have found fragmental genes, but full copies of these fragmented genes were also present in the mitogenome [93]. However, stochasticity aside, we do not have a good explanation for the correlation disappearing only in lineages with double-stranded architectures. In addition, single-stranded mitogenomes exhibited significantly higher architecture and sequence evolutionary rates than double-stranded mitogenomes, and single-stranded architectures were significantly more common in parasitic and low-locomotory lineages. As we did not remove double-stranded mitogenomes that underwent a state reversal, this may have produced some noise in the dataset.

Outliers: There were multiple outliers at the phylum level (Table 1 in the main manuscript). There were also outliers at the class and order levels: (1) GORR was not increased in parasitic lineages in Arachnida (Arthropoda), Enoplea (Nematoda), and Diptera (Arthropoda); (2) GORR was not increased in low-locomotory species in Hexanauplia (Arthropoda).

Nematoda exhibited lower GORR and branch length in single-stranded mitogenomes, and GORR was not increased in parasitic Enoplea. Nematoda was also a major exception in terms of branch length, with endoparasites exhibiting almost identical branch lengths to the free-living species [24]. All Nematoda exhibit relatively low locomotory capacity (Figure S53). Reduced variability in this variable is expected to increase the similarity in evolutionary rates and increase the amount of noise in the dataset. Further, they also exhibit an evolutionary complex mix of parasitic and free-living life histories, with relatively common major life history switches [94]. If the emergence of parasitic lineages is evolutionarily relatively recent, this may further reduce the impact of this variable. Then, according to the definition of parasitism that we relied on in this study, plant-parasitic nematodes were classified as free-living. As they resemble endoparasitic ones in many aspects [24], this can further decrease the impact of this variable. In addition, contrary to the overall bilaterian pattern, nematodes exhibited lower GORR and branch lengths in single-stranded mitogenomes. The two major classes of nematodes differ in this aspect: Enoplea have double-stranded mitogenomes, whereas Chromadorea have single-

stranded mitogenomes [92]. Some of the most highly rearranged architectures were found in the enoplean lineages: Longidoridae, Capillariidae, Trichinellidae, Trichuridae, and Mermithidae (Figure S53), which can explain the outlier partially, but they also indicate that enoplean nematodes have an increased overall level of mitogenomic rearrangements for only partially understood reasons. The unique mitogenomic architectural evolutionary patterns of enoplean nematodes have been observed and discussed before [17,92,95,96].

Diptera (Arthropoda: Insecta) exhibited practically identical GORR values across all four life history categories (Figure S48). As regards the sequence evolution rates, they were the highest in parasitoids, followed by ectoparasites, micropredators, and finally free-living, but all values were similar, so none of the differences was statistically significant [24]. In terms of GORR, it was highly conserved across the entire order (GORR = 3), with only two families exhibiting increased GORR values (Figure S54). Both ectoparasitic families exhibited conserved GORRs. There were only three ectoparasitic species in the dataset, which weakened the statistical analyses. All three species belong to the superfamily Hippoboscoidea: two Streblidae (bat flies) and one Hippoboscidae (*Melophagus ovinus*, sheep ked). Both families exhibit remarkably high locomotory capacity in comparison to most other ectoparasites, aside from fleas, and they resemble micropredators in their lifestyle [24]. In addition, the loss of high locomotory capacity in Hippoboscidae may be of relatively recent evolutionary origin, as sheep ked is an exception within Hippoboscidae for being the only member that has completely lost its wings [97]. Therefore, locomotory capacity appears to be a suitable explanation for this outlier.

Arachnida (Arthropoda) appeared as an outlier in both studies, with ectoparasites exhibiting nonsignificantly shorter branches [24], and GORR values (Figure S47) than the free-living. The analyses were somewhat hampered by the low number of endoparasites (2) in this class, but the number of ectoparasites was rather high (75). Previously, we attributed this outlier (in branch lengths) to a similarity in locomotory capacity between parasitic (ticks) and free-living (mites) lineages [24]. Indeed, herein we also observed that GORR values were strongly increased in arachnids with low locomotory capacity compared to those with high locomotory capacity (Figure S49 and S55).

Hexanauplia (Arthropoda): low-locomotory species exhibited low GORR values (Figure S49 and S56) and branch lengths [24]. This can be attributed to the unique evolution of barnacles (subclass Cirripedia; class Hexanauplia in NCBI's taxonomy database, and Thecostraca in WORMS). There are now multiple lines of evidence across several studies [24,90] indicating that mitogenomes of this lineage are evolving under some of the most stringent purifying selection pressures among all Arthropoda (Figure S56-S57), despite their predominantly sessile lifestyle. Previously, we associated this with a possibility that they exhibit an unusually large N_e [90], but this remains highly questionable, so other explanations should be sought.

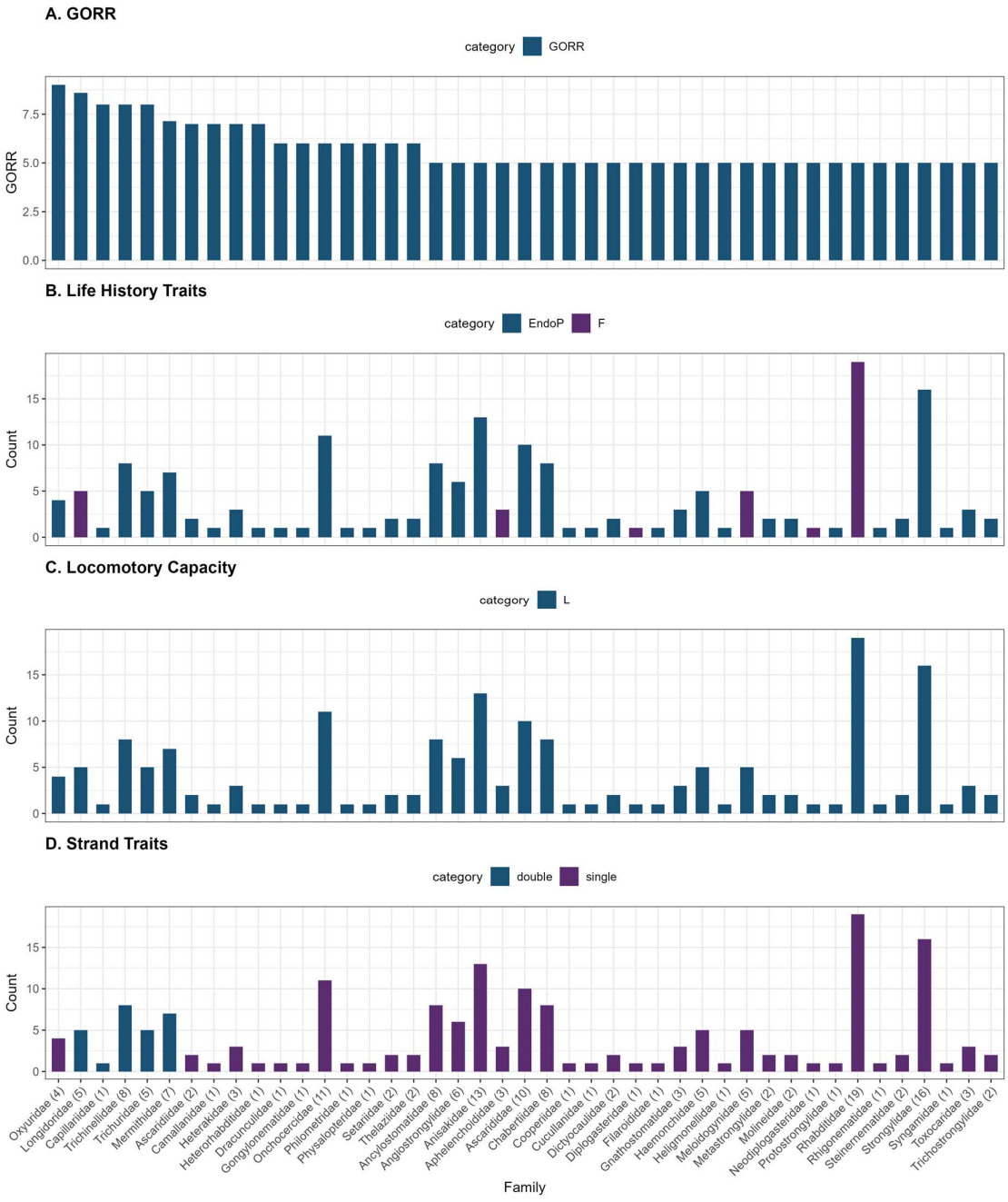

Figure S53. Average GORR values, life history, locomotory capacity, and strandedness across the families of Nematoda. In the life history categorisation, F is free-living, and EndoP is endoparasites. In the locomotory capacity categorisation, L is low. Strandedness categories are double (double-stranded) and single (single-stranded). Families are shown at the bottom, arranged according to the GORR values (high to low), with the number of species included in the dataset shown in brackets.

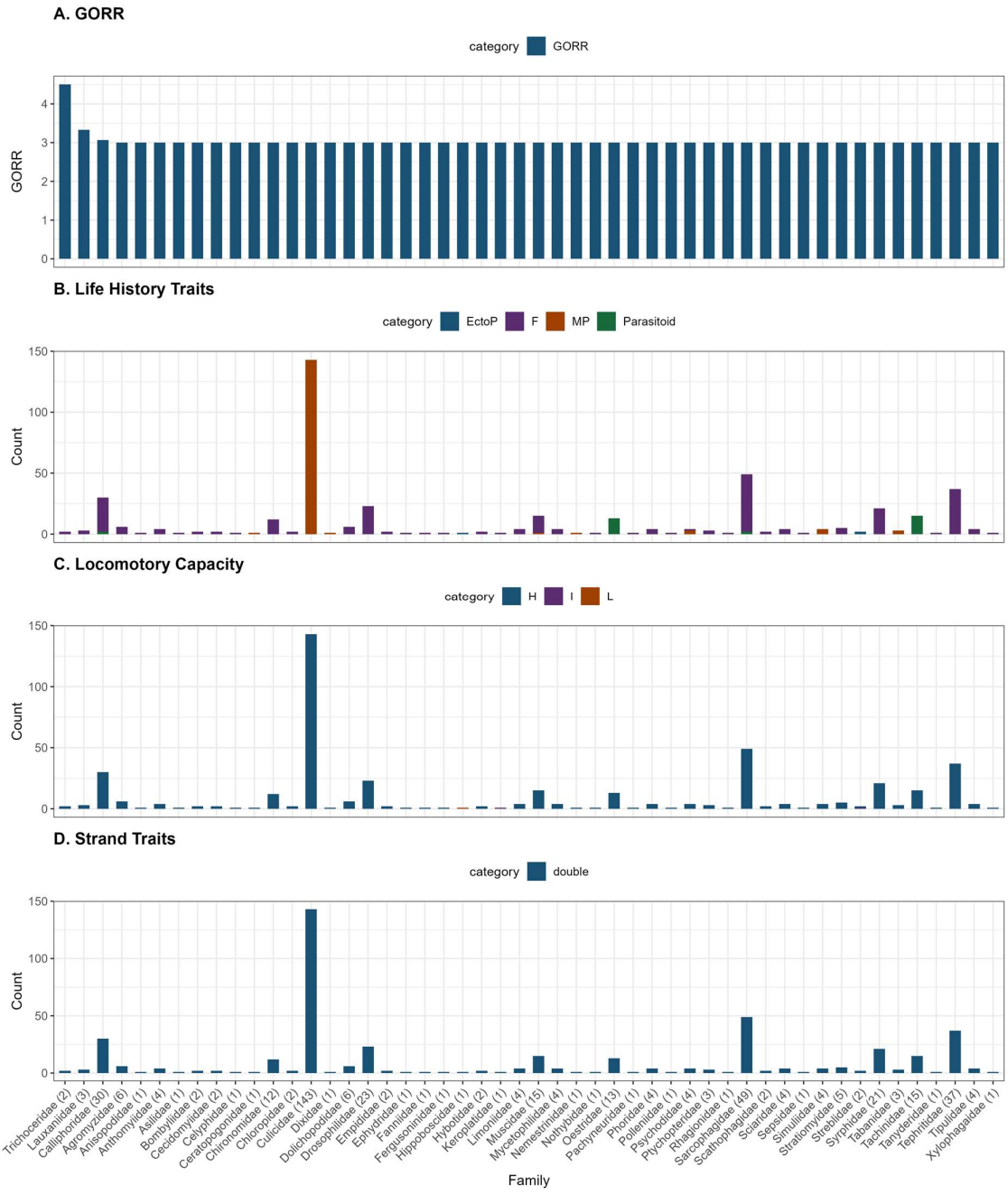

Figure S54. Average GORR values, life history, locomotory capacity, and strandedness across the families of Diptera. In the life history categorisation, F is free-living, EctoP is ectoparasites, and MP is micropredators. In the locomotory capacity categorisation, H is high, I is intermediate, and L is low. All mitogenomes were double-stranded (Strand Traits: double). Families are shown at the bottom, arranged according to the GORR values (high to low), with the number of species included in the dataset shown in brackets.

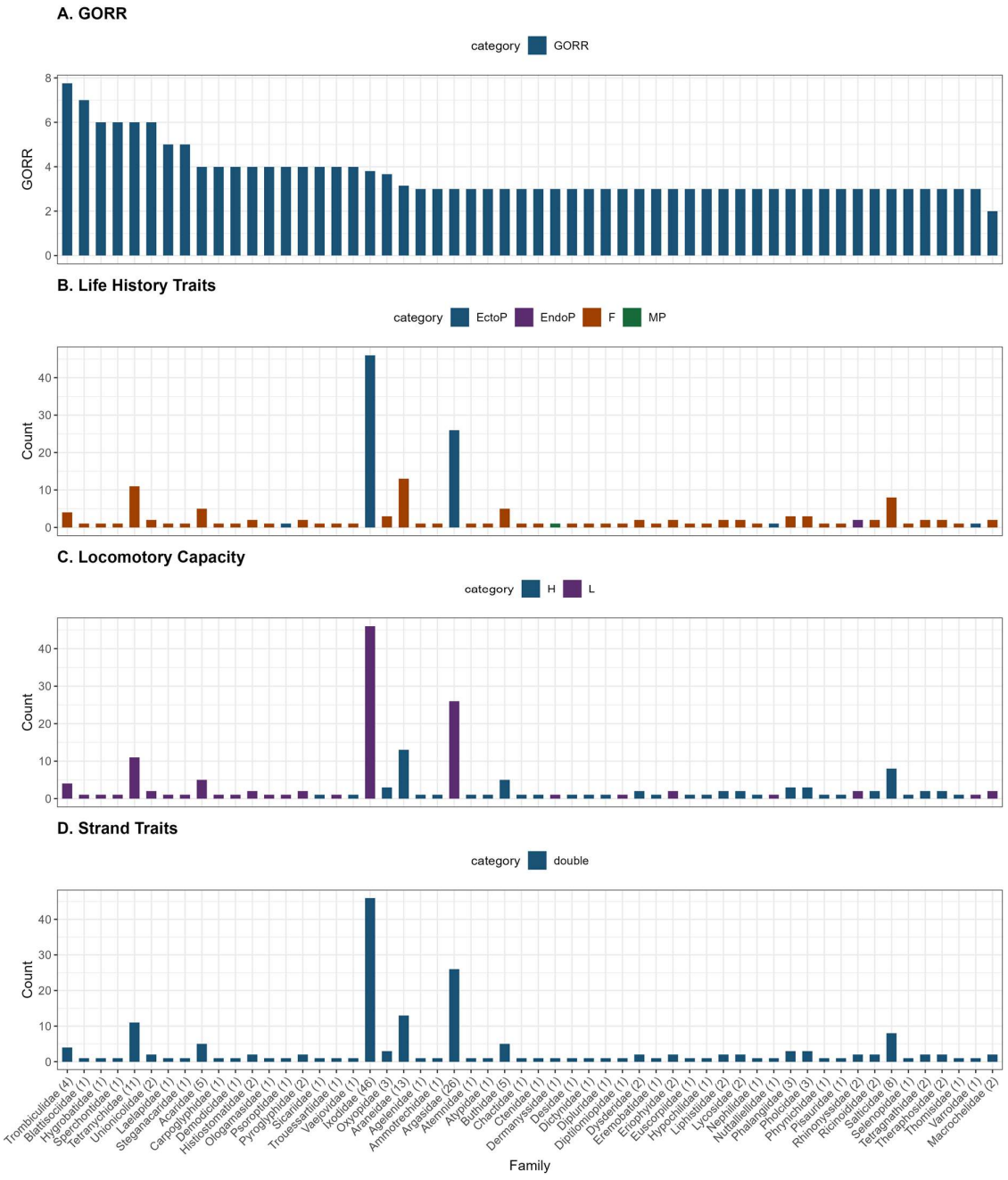

Figure S55. Average GORR values, life history, locomotory capacity, and strandedness across the families of Arachnida. In the life history categorisation, F is free-living, EndoP is endoparasites, EctoP is ectoparasites, and MP is micropredators. In the locomotory capacity categorisation, H is high and L is low. All mitogenomes were double-stranded (Strand Traits: double). Families are shown at the bottom, arranged according to the GORR values (high to low), with the number of species included in the dataset shown in brackets.

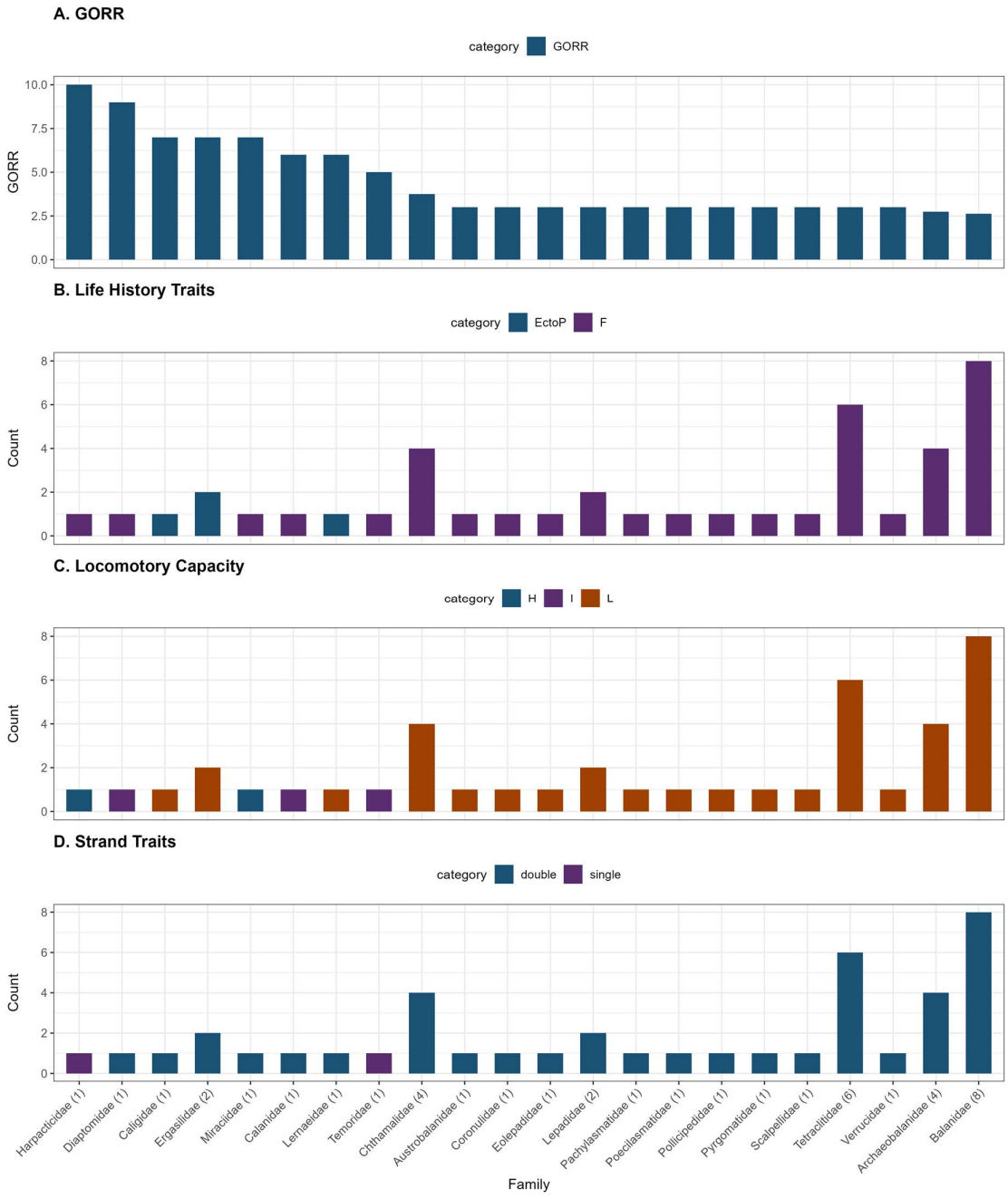

Figure S56. Average GORR values, life history, locomotory capacity, and strandedness across the families of Hexanauplia (Arthropoda). In the life history categorisation, F is free-living, EndoP is endoparasites, EctoP is ectoparasites, and MP is micropredators. In the locomotory capacity categorisation, H is high and L is low. All mitogenomes were double-stranded (Strand Traits: double). Families are shown at the bottom, arranged according to the GORR values (high to low), with the number of species included in the dataset shown in brackets.

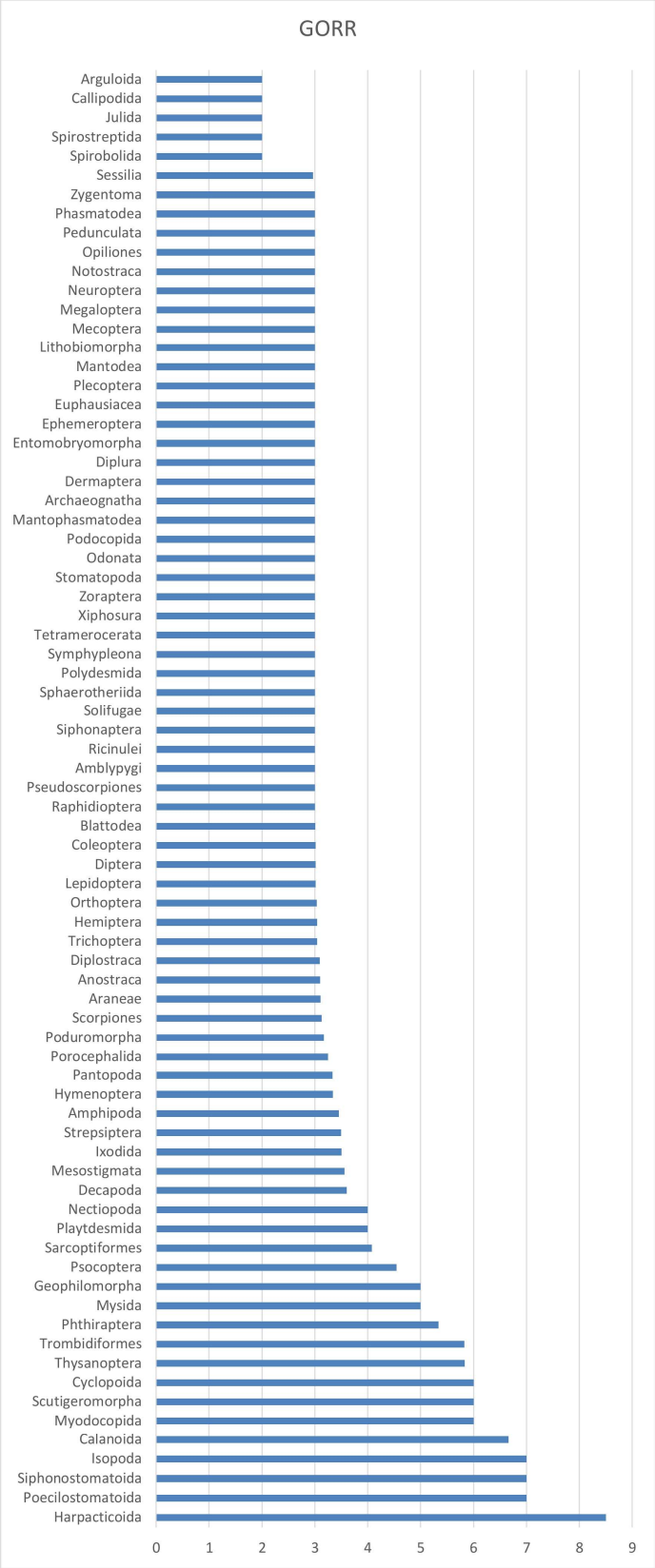
GORR
Arguloida
Callipodida
Julida
Spirostreptida
Spirobolida
Sessilia
Zygentoma
Phasmatodea
Pedunculata
Opiliones
Notostraca
Neuroptera
Megaloptera
Mecoptera
Lithobiomorpha
Mantodea
Plecoptera
Euphausiacea
Ephemeroptera
Entomobryomorpha
Diplura
Dermaptera
Archaeognatha
Mantophasmatodea
Podocopida
Odonata
Stomatopoda
Zoraptera
Xiphosura
Tetramerocerata
Symphypleona
Polydesmida
Sphaerotheriida
Solifugae
Siphonaptera
Ricinulei
Amblypygi
Pseudoscorpiones
Raphidioptera
Blattodea
Coleoptera
Diptera
Lepidoptera
Orthoptera
Hemiptera
Trichoptera
Diplostraca
Anostraca
Araneae
Scorpiones
Poduromorpha
Porocephalida
Pantopoda
Hymenoptera
Amphipoda
Strepsiptera
Ixodida
Mesostigmata
Decapoda
Nectiopoda
Playtdesmida
Sarcoptiformes
Psocoptera
Geophilomorpha
Mysida
Phthiraptera
Trombidiformes
Thysanoptera
Cyclopoida
Scutigeromorpha
Myodocopida
Calanoida
Isopoda
Siphonostomatoida
Poecilostomatoida
Harpacticoida
0
1
2
3
4
5
6
7
8
9

Figure S57. Average GORR values across the orders of Arthropoda.

References

1. Zhang, D. *et al.* Mitochondrial genomes and 28S rDNA contradict the proposed obsoletion of the order Tetraonchidea (Platyhelminthes: Monogenea). *International Journal of Biological Macromolecules* **143**, 891–901 (2020).

2. Zhang, D. *et al.* Evidence for Adaptive Selection in the Mitogenome of a Mesoparasitic Monogenean Flatworm Enterogyrus malmbergi. *Genes* **10**, 863 (2019).

3. Zhang, D. *et al.* Mitochondrial genomes of two diplectanids (Platyhelminthes: Monogenea) expose paraphyly of the order Dactylogyridea and extensive tRNA gene rearrangements. *Parasites & Vectors* **11**, 601 (2018).

4. Zhang, D. *et al.* Three new Diplozoidae mitogenomes expose unusual compositional biases within the Monogenea class: implications for phylogenetic studies. *BMC Evolutionary Biology* **18**, 133 (2018).

5. Zhang, D. *et al.* Sequencing of the complete mitochondrial genome of a fish-parasitic flatworm Paratetraonchoides inermis (Platyhelminthes: Monogenea): tRNA gene arrangement reshuffling and implications for phylogeny. *Parasites & Vectors* **10**, 462 (2017).

6. Zhang, D. *et al.* Sequencing, characterization and phylogenomics of the complete mitochondrial genome of Dactylogyrus lamellatus (Monogenea: Dactylogyridae). *Journal of Helminthology* 1–12 (2017) doi:10.1017/S0022149X17000578.

7. Zhang, D. *et al.* Mitochondrial Genomes of Two Thaparocleidus Species (Platyhelminthes: Monogenea) Reveal the First rRNA Gene Rearrangement among the Neodermata. *International Journal of Molecular Sciences* **20**, 4214 (2019).

8. Zhang, D. *et al.* Homoplasy or plesiomorphy? Reconstruction of the evolutionary history of mitochondrial gene order rearrangements in the subphylum Neodermata. *International Journal for Parasitology* **49**, 819–829 (2019).

9. Li, W. X. *et al.* Characterization and phylogenomics of the complete mitochondrial genome of the polyzoic cestode Gangesia oligonchis (Platyhelminthes: Onchoproteocephalidea). *Journal of Helminthology* **94**, e58 (2020).

10. Li, W. X. *et al.* The complete mitochondrial DNA of three monozoic tapeworms in the Caryophyllidea: a mitogenomic perspective on the phylogeny of eucestodes. *Parasites & Vectors* **10**, 314 (2017).

11. Li, W. X. *et al.* Comparative mitogenomics supports synonymy of the genera Ligula and Digramma (Cestoda: Diphyllobothriidae). *Parasites & Vectors* **11**, 324 (2018).

12. Zou, H. *et al.* The complete mitochondrial genome of Gyrodactylus gurleyi (Platyhelminthes: Monogenea). *Mitochondrial DNA Part B* **1**, 383–385 (2016).

13. Lei, H.-P. *et al.* Geography, phylogeny and host switch drive the coevolution of parasitic Gyrodactylus flatworms and their hosts. *Parasites Vectors* **17**, 42 (2024).

14. Zhang, D. *et al.* Strong mitonuclear discordance in the phylogeny of Neodermata and evolutionary rates of Polyopisthocotylea. *Int J Parasitol* **54**, 213–223 (2024).

15. Zhang, D. *et al.* The complete mitochondrial genome of Gyrodactylus kobayashii (Platyhelminthes: Monogenea). *Mitochondrial DNA B Resour* **1**, 146–147 (2016).

16. Hu, Y. *et al.* Complete mitochondrial genome and phylogenetic analysis of Dollfustrema vaneyi (Trematoda: Bucephalidae). *BMC Genomics* **25**, 862 (2024).

17. Zou, H. *et al.* Inverted base composition skews and discontinuous mitochondrial genome architecture evolution in the Enoplea (Nematoda). *BMC Genomics* **23**, 376 (2022).

18. Zou, H. *et al.* Evolutionary rates of mitochondrial sequences and gene orders in Spirurina (Nematoda) are episodic but synchronised. *Water Biology and Security* **1**, 100033 (2022).

19. Zou, H. *et al.* The complete mitochondrial genome of parasitic nematode Camallanus cotti: extreme discontinuity in the rate of mitogenomic architecture evolution within the Chromadorea class. *BMC Genomics* **18**, 840 (2017).

20. Chen, F. *et al.* Sequencing of the Complete Mitochondrial Genome of Pingus sinensis (Spirurina: Quimperiidae): Gene Arrangements and Phylogenetic Implications. *Genes* **12**, 1772 (2021).

21. Zou, H. *et al.* The complete mitochondrial genome of Cymothoa indica has a highly rearranged gene order and clusters at the very base of the Isopoda clade. *PLOS ONE* **13**, e0203089 (2018).

22. Zou, H. *et al.* Architectural instability, inverted skews and mitochondrial phylogenomics of Isopoda: outgroup choice affects the long-branch attraction artefacts. *Royal Society Open Science* **7**, 191887 (2020).

23. Hua, C. J. *et al.* Basal position of two new complete mitochondrial genomes of parasitic Cymothoida (Crustacea: Isopoda) challenges the monophyly of the suborder and phylogeny of the entire order. *Parasites & Vectors* **11**, 628 (2018).

24. Jakovlić, I. *et al.* Mitogenomic evolutionary rates in Bilateria are influenced by parasitic lifestyle and locomotory capacity. *Nat Commun* **14**, 6307 (2023).

25. Xiang, C. *et al.* Using PhyloSuite for molecular phylogeny and tree-based analyses. *iMeta* **2**, e87 (2023).

26. Lafferty, K. D. *et al.* A general consumer-resource population model. *Science* **349**, 854–857 (2015).

27. Weinstein, S. B. & Kuris, A. M. Independent origins of parasitism in Animalia. *Biology Letters* **12**, 20160324 (2016).

28. Childress, J. J. & Mickel, T. J. Metabolic rates of animals from the hydrothermal vents and other deep-sea habitats. *Bulletin of The Biological Society of Washington* **6**, 249–260 (1985).

29. Seibel, B. A. & Drazen, J. C. The rate of metabolism in marine animals: environmental constraints, ecological demands and energetic opportunities. *Philosophical Transactions of the Royal Society B: Biological Sciences* **362**, 2061–2078 (2007).

30. Zhang, D. *et al.* PhyloSuite: an integrated and scalable desktop platform for streamlined molecular sequence data management and evolutionary phylogenetics studies. *Molecular Ecology Resources* **20**, 348–355 (2020).

31. Katoh, K. & Standley, D. M. MAFFT multiple sequence alignment software version 7: Improvements in performance and usability. *Molecular Biology and Evolution* **30**, 772–780 (2013).

32. Capella-Gutiérrez, S., Silla-Martínez, J. M. & Gabaldón, T. trimAl: a tool for automated alignment trimming in large-scale phylogenetic analyses. *Bioinformatics* **25**, 1972–1973 (2009).

33. Perrin, A., Varré, J.-S., Blanquart, S. & Ouangraoua, A. ProCARs: Progressive Reconstruction of Ancestral Gene Orders. *BMC Genomics* **16**, S6 (2015).

34. Webster, B. L. *et al.* Mitogenomics and phylogenomics reveal priapulid worms as extant models of the ancestral Ecdysozoan. *Evolution & Development* **8**, 502–510 (2006).

35. Kapli, P. *et al.* Lack of support for Deuterostomia prompts reinterpretation of the first Bilateria. *Science Advances* **7**, eabe2741 (2021).

36. Kapli, P. & Telford, M. J. Topology-dependent asymmetry in systematic errors affects phylogenetic placement of Ctenophora and Xenacoelomorpha. *Science Advances* **6**, eabc5162 (2020).

37. O'Leary, N. A. *et al.* Reference sequence (RefSeq) database at NCBI: Current status, taxonomic expansion, and functional annotation. *Nucleic Acids Research* **44**, D733–D745 (2016).

38. Lavrov, D. V. & Lang, B. F. Poriferan mtDNA and Animal Phylogeny Based on Mitochondrial Gene Arrangements. *Syst Biol* **54**, 651–659 (2005).

39. Oxusoff, L., Préa, P. & Perez, Y. A complete logical approach to resolve the evolution and dynamics of mitochondrial genome in bilaterians. *PLOS ONE* **13**, e0194334 (2018).

40. Bourlat, S. J., Rota-Stabelli, O., Lanfear, R. & Telford, M. J. The mitochondrial genome structure of Xenoturbella bocki (phylum Xenoturbellida) is ancestral within the deuterostomes. *BMC Evolutionary Biology* **9**, 107 (2009).

41. Staton, J. L., Daehler, L. L. & Brown, W. M. Mitochondrial gene arrangement of the horseshoe crab Limulus polyphemus L.: conservation of major features among arthropod classes. *Molecular Biology and Evolution* **14**, 867–874 (1997).

42. Podsiadlowski, L., Braband, A., Struck, T. H., von Döhren, J. & Bartolomaeus, T. Phylogeny and mitochondrial gene order variation in Lophotrochozoa in the light of new mitogenomic data from Nemertea. *BMC Genomics* **10**, 364 (2009).

43. Shtolz, N. & Mishmar, D. The metazoan landscape of mitochondrial DNA gene order and content is shaped by selection and affects mitochondrial transcription. *Commun Biol* **6**, 1–15 (2023).

44. Babbucci, M., Basso, A., Scupola, A., Patarnello, T. & Negrisolo, E. Is It an Ant or a Butterfly? Convergent Evolution in the Mitochondrial Gene Order of Hymenoptera and Lepidoptera. *Genome Biology and Evolution* **6**, 3326–3343 (2014).

45. Struck, T. H., Golombek, A., Hoesel, C., Dimitrov, D. & Elgetany, A. H. Mitochondrial Genome Evolution in Annelida—A Systematic Study on Conservative and Variable Gene Orders and the Factors Influencing its Evolution. *Systematic Biology* **72**, 925–945 (2023).

46. Boore, J. L. The use of genome-level characters for phylogenetic reconstruction. *Trends in Ecology and Evolution* **21**, 439–446 (2006).

47. Bernt, M. *et al.* A comprehensive analysis of bilaterian mitochondrial genomes and phylogeny. *Molecular Phylogenetics and Evolution* **69**, 352–364 (2013).

48. Singh, T. R. *et al.* Tunicate mitogenomics and phylogenetics: peculiarities of the Herdmania momus mitochondrial genome and support for the new chordate phylogeny. *BMC Genomics* **10**, 534 (2009).

49. Bliznina, A. *et al.* Telomere-to-telomere assembly of the genome of an individual Oikopleura dioica from Okinawa using Nanopore-based sequencing. *BMC Genomics* **22**, 222 (2021).

50. Denoeud, F. *et al.* Plasticity of Animal Genome Architecture Unmasked by Rapid Evolution of a Pelagic Tunicate. *Science* **330**, 1381–1385 (2010).

51. Dierckxsens, N. *et al.* Tracing Homopolymers in Oikopleura dioica's Mitogenome. *Genome Biology and Evolution* **16**, evae182 (2024).

52. Klirs, Y. *et al.* Evolutionary Insights from the Mitochondrial Genome of Oikopleura dioica: Sequencing Challenges, RNA Editing, Gene Transfers to the Nucleus, and tRNA Loss. *Genome Biology and Evolution* **16**, evae181 (2024).

53. Delsuc, F. *et al.* A phylogenomic framework and timescale for comparative studies of tunicates. *BMC Biology* **16**, 39 (2018).

54. Wibisana, J. N. *et al.* The complete mitogenome of an unidentified *Oikopleura* species. Preprint at https://doi.org/10.12688/f1000research.157311.2 (2025).

55. Joo, S., Lee, J., Lee, D.-Y., Xi, H. & Park, J. The complete mitochondrial genome of the millipede Epanerchodus koreanus Verhoeff, 1937 collected in limestone cave of Korea (Polydesmidae: Polydesmida). *Mitochondrial DNA. Part B, Resources* **5**, 3845 (2020).

56. Brewer, M. S., Swafford, L., Spruill, C. L. & Bond, J. E. Arthropod Phylogenetics in Light of Three Novel Millipede (Myriapoda: Diplopoda) Mitochondrial Genomes with Comments on the

Appropriateness of Mitochondrial Genome Sequence Data for Inferring Deep Level Relationships. *PLOS ONE* **8**, e68005 (2013).

57. Blanco-Bercial, L., Bradford-Grieve, J. & Bucklin, A. Molecular phylogeny of the Calanoida (Crustacea: Copepoda). *Molecular Phylogenetics and Evolution* **59**, 103–113 (2011).

58. Choi, B.-S. *et al.* Complete mitochondrial genome of the calanoid copepod Eurytemora affinis (Calanoida, Temoridae). *Mitochondrial DNA Part B* **4**, 2731–2733 (2019).

59. Burton, R., Byrne, R. & Rawson, P. Three divergent mitochondrial genomes from California populations of the copepod Tigriopus californicus. *Gene* **403**, 53–9 (2007).

60. Boore, J. L. & Brown, W. M. Complete DNA sequence of the mitochondrial genome of the black chiton, Katharina tunicata. *Genetics* **138**, 423–443 (1994).

61. Helfenbein, K. G. & Boore, J. L. The Mitochondrial Genome of Phoronis architecta—Comparisons Demonstrate that Phoronids Are Lophotrochozoan Protostomes. *Molecular Biology and Evolution* **21**, 153–157 (2004).

62. Laumer, C. E. *et al.* Revisiting metazoan phylogeny with genomic sampling of all phyla. *Proceedings of the Royal Society B: Biological Sciences* **286**, 20190831 (2019).

63. Kocot, K. M. *et al.* Phylogenomics of Lophotrochozoa with Consideration of Systematic Error. *Systematic Biology* **66**, 256–282 (2017).

64. Halanych, K. M. Lophotrochozoa, Diversification of. in *Encyclopedia of Ecolutionary Biology* 405–408 (Elsevier, 2016). doi:10.1016/B978-0-12-800049-6.00272-9.

65. Egger, B. *et al.* A Transcriptomic-Phylogenomic Analysis of the Evolutionary Relationships of Flatworms. *Current Biology* **25**, 1347–1353 (2015).

66. Laumer, C. E., Hejnol, A. & Giribet, G. Nuclear genomic signals of the 'microturbellarian' roots of platyhelminth evolutionary innovation. *eLife* **4**, e05503 (2015).

67. Rosa, M. T., Oliveira, D. S. & Loreto, E. L. S. Characterization of the first mitochondrial genome of a catenulid flatworm: Stenostomum leucops (Platyhelminthes). *Journal of Zoological Systematics and Evolutionary Research* **55**, 98–105 (2017).

68. Grant, H. E. *et al.* Multiple evolutionary transitions of reproductive strategies in a phylum of aquatic colonial invertebrates. *Proceedings of the Royal Society B: Biological Sciences* **290**, 20231458 (2023).

69. Weigert, A. & Bleidorn, C. Current status of annelid phylogeny. *Org Divers Evol* **16**, 345–362 (2016).

70. Mikhailov, K. V. *et al.* The Genome of Intoshia linei Affirms Orthonectids as Highly Simplified Spiralians. *Current Biology* **26**, 1768–1774 (2016).

71. Daffe, G., Sun, Y., Ahyong, S. T. & Kupriyanova, E. K. Mitochondrial genome of Sabella spallanzanii (Gmelin, 1791) (Sabellida: Sabellidae). *Mitochondrial DNA Part B* **6**, 499–501 (2021).

72. Kocot, K. M. *et al.* Phylogenomics reveals deep molluscan relationships. *Nature* **477**, 452–456 (2011).

73. Chen, Z. *et al.* A genome-based phylogeny for Mollusca is concordant with fossils and morphology. *Science* **387**, 1001–1007 (2025).

74. Bergmeier, F. S. *et al.* Complementing aculiferan mitogenomics: comparative characterization of mitochondrial genomes of Solenogastres (Mollusca, Aplacophora). *BMC Ecology and Evolution* **24**, 128 (2024).

75. Stöger, I. *et al.* Monoplacophoran mitochondrial genomes: convergent gene arrangements and little phylogenetic signal. *BMC Evolutionary Biology* **16**, 274 (2016).

76. Li, Y.-X. *et al.* Phylogenomics of Bivalvia Using Ultraconserved Elements Reveal New Topologies for Pteriomorphia and Imparidentia. *Systematic Biology* syae052 (2024) doi:10.1093/sysbio/syae052.

77. Sharma, P. P. *et al.* Into the deep: A phylogenetic approach to the bivalve subclass Protobranchia. *Molecular Phylogenetics and Evolution* **69**, 188–204 (2013).

78. Lee, Y. *et al.* A mitochondrial genome phylogeny of Mytilidae (Bivalvia: Mytilida). *Molecular Phylogenetics and Evolution* **139**, 106533 (2019).

79. Zhang, K., Sun, J., Xu, T., Qiu, J.-W. & Qian, P.-Y. Phylogenetic Relationships and Adaptation in Deep-Sea Mussels: Insights from Mitochondrial Genomes. *International Journal of Molecular Sciences* **22**, 1900 (2021).

80. Robicheau, B. M., Breton, S. & Stewart, D. T. Sequence motifs associated with paternal transmission of mitochondrial DNA in the horse mussel, Modiolus modiolus (Bivalvia: Mytilidae). *Gene* **605**, 32–42 (2017).

81. Zhu, Y. *et al.* Comparative mitochondrial genome analysis provides new insights into the classification of Modiolinae. *Mol Biol Rep* **51**, 823 (2024).

82. Audino, J. A., Serb, J. M. & Marian, J. E. A. R. Phylogeny and anatomy of marine mussels (Bivalvia: Mytilidae) reveal convergent evolution of siphon traits. *Zoological Journal of the Linnean Society* **190**, 592–612 (2020).

83. Passamonti, M., Ricci, A., Milani, L. & Ghiselli, F. Mitochondrial genomes and Doubly Uniparental Inheritance: new insights from Musculista senhousia sex-linked mitochondrial DNAs (Bivalvia Mytilidae). *BMC Genomics* **12**, 442 (2011).

84. Weigert, A. *et al.* Evolution of mitochondrial gene order in Annelida. *Molecular Phylogenetics and Evolution* **94**, 196–206 (2016).

85. Vasilikopoulos, A. *et al.* Whole-genome analyses converge to support the Hemirotifera hypothesis within Syndermata (Gnathifera). *Hydrobiologia* **851**, 2795–2826 (2024).

86. Herlyn, H. *et al.* Substantial hierarchical reductions of genetic and morphological traits in the evolution of rotiferan parasites. 2024.08.01.605096 Preprint at https://doi.org/10.1101/2024.08.01.605096 (2024).

87. Suga, K., Mark Welch, D. B., Tanaka, Y., Sakakura, Y. & Hagiwara, A. Two circular chromosomes of unequal copy number make up the mitochondrial genome of the rotifer Brachionus plicatilis. *Molecular Biology and Evolution* **25**, 1129–1137 (2008).

88. Golombek, A., Tobergte, S. & Struck, T. H. Elucidating the phylogenetic position of Gnathostomulida and first mitochondrial genomes of Gnathostomulida, Gastrotricha and Polycladida (Platyhelminthes). *Molecular Phylogenetics and Evolution* **86**, 49–63 (2015).

89. Bondarenko, N., Bondarenko, A., Starunov, V. & Slyusarev, G. Comparative analysis of the mitochondrial genomes of Orthonectida: insights into the evolution of an invertebrate parasite species. *Mol Genet Genomics* **294**, 715–727 (2019).

90. Jakovlić, I. *et al.* Slow crabs - fast genomes: locomotory capacity predicts skew magnitude in crustacean mitogenomes. *Molecular Ecology* **30**, 5488–5502 (2021).

91. Jakovlić, I. *et al.* Evolutionary history of inversions in directional mutational pressures in crustacean mitochondrial genomes: Implications for evolutionary studies. *Molecular Phylogenetics and Evolution* **164**, 107288 (2021).

92. Gissi, C., Iannelli, F. & Pesole, G. Evolution of the mitochondrial genome of Metazoa as exemplified by comparison of congeneric species. *Heredity* **101**, 301–320 (2008).

93. Zou, H. *et al.* The complete mitochondrial genome of parasitic nematode Camallanus cotti: extreme discontinuity in the rate of mitogenomic architecture evolution within the Chromadorea class. *BMC Genomics* **18**, 840 (2017).

94. Blaxter, M. & Koutsovoulos, G. The evolution of parasitism in Nematoda. *Parasitology* **142**, S26–S39 (2015).

95. Lavrov, D. V. & Brown, W. M. Trichinella spiralis mtDNA: A nematode mitochondrial genome that encodes a putative ATP8 and normally structured tRNAs and has a gene arrangement relatable to those of coelomate metazoans. *Genetics* **157**, 621–637 (2001).

96. Hyman, B. C., Lewis, S. C., Tang, S. & Wu, Z. Rampant gene rearrangement and haplotype hypervariation among nematode mitochondrial genomes. *Genetica* **139**, 611–615 (2011).

97. Small, R. W. A review of Melophagus ovinus (L.), the sheep ked. *Veterinary Parasitology* **130**, 141–155 (2005).